

DESIGN AND DEVELOPMENT OF PVDF HYDROPHONE FOR UNDERWATER APPLICATION



By

Muhammad Huzaifa

(Registration No: 00000431970)

Supervised by

Dr. Anas Bin Aqeel

Department of Mechatronics Engineering (DMTS)

College of Electrical and Mechanical Engineering (CEME)

National University of Sciences & Technology (NUST)

Islamabad, Pakistan (2024)


THESIS ACCEPTANCE CERTIFICATE

Certified that final copy of MS/MPhil thesis by Mr. PN Muhammad Huzaifa Registration No. 00000431970, of Electrical and Mechanical Engineering College has been vetted by undersigned, found complete in all respects as per NUST Statues/Regulations, is free of plagiarism, errors, and mistakes and is accepted as partial fulfillment for award of MS/MPhil degree. It is further certified that necessary amendments as pointed out by GEC members of the scholar have also been incorporated in the said thesis.

Signature: 

Name of Supervisor: Dr Anas Bin Aqeel

Dated: 27 Sep 2024

Signature of HOD: 

Dr. Hamid Jabbar

Date: 27 Sep 2024

Signature of Dean: 

Brig Dr. Nasir Rashid

Date: 27 SEP 2024

DEDICATION

This thesis is dedicated to my beloved son, M Yahya, and my wonderful wife. A special thanks to my wife for her unwavering support throughout my master's journey, especially during the completion of this thesis. I am also deeply grateful to my parents, whose constant prayers made this achievement possible. Without their love and blessings, this journey would not have been fulfilled.

ACKNOWLEDGEMENTS

I would like to start by thanking all the teachers who taught me during my MS coursework. Their dedication and knowledge helped me build a strong foundation for my studies. A special thanks goes to Dr. Hamid Jabbar, Head of Department, who taught me Data Acquisition and Controls. He was the one who encouraged and motivated me to focus my thesis on the field of piezoelectric materials, and for that, I am truly grateful.

I am also deeply thankful to Dr. Hassan Elahi for his constant support and guidance throughout my thesis. His deep understanding of piezoelectric materials and his help with solving problems, especially in simulations, were vital to my research. His encouragement kept me going, and without his moral support, I would have struggled to complete my thesis on time.

I would also like to express my sincere thanks to my supervisor, Dr. Anas Bin Aqeel, for his valuable advice and thoughtful feedback. His critical thinking helped me approach my research in new and creative ways, which greatly improved the quality of my work. I am grateful to my friends, colleagues, and all the seniors and juniors in the MNRT Lab who helped me along the way. Their support, whether in discussions or providing help when needed, made a big difference during my thesis journey. Lastly, I want to thank my family, especially my parents, whose prayers and support kept me going through this journey. My friends also deserve a big thank you for being there for me during both the good and challenging times. Without all of you, this journey would not have been possible.

ABSTRACT

In recent years, underwater acoustic measurement has gained significant importance due to the increasing need for detecting and monitoring underwater objects such as marine life and vehicles. Acoustic waves remain the most efficient method for transmitting information across long distances underwater. Consequently, extensive research has been directed towards the development of hydrophones and acoustic sensors that can address the requirements of diverse underwater applications and conditions. These devices are crucial in areas like marine biology, underwater exploration, and naval defense. Efforts are being made by researchers to enhance the precision and dependability of these sensors to ensure optimal performance across various underwater settings. Continuous progress in this technology is enhancing our ability to understand and engage with the underwater realm.

Polyvinylidene fluoride (PVDF) film stands out among acoustic sensing materials due to its remarkable piezoelectric characteristics and acoustic impedance, which closely matches that of water. PVDF possesses attributes that make it an excellent choice for underwater acoustic sensors. Although PVDF is commonly used in hydrophone applications, its exact sensing mechanism in underwater sound environments is not yet completely understood. This thesis aims to explore the behavior of PVDF film in underwater sound fields and leverage the findings to design both a hydrophone and an acoustic vector sensor using PVDF.

Recent progress in underwater acoustic sensors has been driven by the growing need for improved detection and localization in underwater operations, such as acoustic noise monitoring, target identification, and object tracking. Acoustic waves, capable of traveling over long distances underwater, are significantly more effective for communication and sensing in aquatic environments

compared to electromagnetic waves. To enhance these abilities, a new Micro-Electro-Mechanical System (MEMS) has been developed, inspired by the auditory functions of a bionic fish's lateral line organ. This system includes a piezoelectric polymer-based acoustic vector hydrophone made from PVDF, which captures vector information from the underwater acoustic sound field.

PVDF is a highly suitable material for underwater applications due to its flat frequency response, excellent mechanical flexibility, and ideal acoustic impedance. This study concentrates on the design and analysis of a PVDF-based hydrophone sensor, with its performance validated using analytical models. The hydrophone has been optimized through simulation and parametric sweeps, showing notable improvements in its functionality. The findings indicate that the vector hydrophone offers a flat frequency response and optimal sensitivity, especially for detecting the direction of low-frequency acoustic waves. These characteristics are crucial for various underwater applications, including sonar systems and navigation.

The sensor's performance shows a marked improvement over previous models, with sensitivity enhanced by 5 dB, achieving a sensitivity level of -186 dB and a frequency bandwidth ranging from 20 Hz to 1.5 kHz ($0 \text{ dB} = 1 \text{ V}/\mu\text{Pa}$). These findings highlight the advancements made by the novel PVDF hydrophone, offering improved detection capabilities and accuracy for low-frequency sound waves in underwater environments. This represents a significant step forward in the field of underwater acoustic sensing technology.

. **Keywords:** MEMS, piezoelectric polymer, acoustic vector hydrophone, PVDF, underwater sensing, Low frequency, MEMS

TABLE OF CONTENTS

ACKNOWLEDGEMENTS	III
ABSTRACT	IV
TABLE OF CONTENTS	VII
LIST OF TABLES	IX
LIST OF FIGURES	XI
LIST OF SYMBOLS, ABBREVIATIONS AND ACRONYMS	XII
CHAPTER 1: INTRODUCTION	1
1.1 General Background and Motivation	1
1.2 Performance Metrics	3
1.2.1 Sensitivity	3
1.2.2 Frequency Response (Bandwidth)	4
1.2.3 Directional Response (Directivity)	5
1.2.4 Active Size Element	6
1.2.5 Acoustic Impedance	7
1.3 Mems Underwater Hydrophone	8
1.4 Problem Statement	9
1.5 Research Objectives	10
1.6 Methodology	10
CHAPTER 2: LITERATURE REVIEW	11
2.1 Underwater Hydrophone	11
2.2 Types of Hydrophones	12
2.2.1 Scaler Hydrophone	12
2.2.2 Vector Hydrophone	13
2.3 Underwater Acoustic Vector Sensors	14

2.4	PVDF Polymer	14
2.5	PVDF film as an underwater acoustic sensor	16
CHAPTER 3: WORKING PRINCIPLE OF HYDROPHONE		18
3.1	Cilia-Type Four-Beam Vector Hydrophone	18
3.1.1	Bionic Principle of The Sensor	19
3.2	Direction Detector Model of Acoustic Wave	21
3.2.1	Direction Detection Principle	21
CHAPTER 4: SENSING MECHANISM OF A PVDF HYDROPHONE		25
4.1	Piezoelectric Effect and Its Constitutive Equations	25
4.1.1	Constitutive Equations for The Sensing Mode	26
4.1.2	Constitutive Equations for The Actuation Mode	28
CHAPTER 5: HYDROPHONE OPERATING MECHANISM		29
5.1	Operating at the Resonance Frequency	29
5.2	Hydrophones Operation for Low-Frequency Applications	31
5.3	Mathematical modeling of piezoelectric sensor	32
CHAPTER 6: FEM ANALYSIS OF UNDERWATER HYDROPHONE		35
6.1	Structural Analysis without FSI	37
6.2	Structural Analysis with FSI	40
CHAPTER 7 RESULTS AND DISCUSSIONS		43
7.1	Parametric Scans of Design Parameters	43
7.1.1	Thickness of the Cantilever Beam	44
7.1.2	Height of the Vertical Cilium	47
7.1.3	Pressure VS Displacement (shape of active size element):	50
7.1.3.1	Rectangular Shape	50
7.1.3.2	Circular Shape	51
CHAPTER 8: CONCLUSION AND FUTURE WORK		53
8.1	Conclusion	53

REFERNCES

LIST OF PUBLICATIONS AND PATENTS

LIST OF TABLES

Table 1.1: Comparison of Piezoelectric Properties	3
Table 2.1: Material Analysis of PVDF Disc	15
Table 3.1: Material Properties of the Material	19
Table 6.1: Non FSI Voltage and Displacement Response	38
Table 6.2: FSI Voltage and Displacement Response	40

LIST OF FIGURES

Figure 1.1: Active Size Element (Vertical Cilium)	7
Figure 3.1: Cilia Four Beam Vector Hydrophone	18
Figure 3.2: (a) Schematic drawing of fish lateral line (b) neuromast organ	20
Figure 3.3: Sense-conducting pathway of a fish's lateral line organ	21
Figure 3.4: The projection in the rectangular coordinate system of the wave vector	22
Figure 4.1: Schematic drawing of the (a) direct, (b) converse piezoelectric effect	25
Figure 4.2: Piezoelectricity in both sensing mode	27
Figure 4.3: Piezoelectricity in both actuation mode	28
Figure 6.1: Vector hydrophone structure	36
Figure 6.2: Modal analysis of vector hydrophone structure	39
Figure 6.3: Wet (FSI) modal analysis of vector hydrophone structure	41
Figure 7.1: Stationary analysis (Thickness VS Voltage)	44
Figure 7.2: Modal Analysis (Thickness VS Frequency)	45
Figure 7.3: Sensitivity Analysis (Frequency VS Sensitivity)	46
Figure 7.4: Stationary analysis (Height VS Voltage)	47
Figure 7.5: Modal analysis (Height VS Freq)	48
Figure 7.6: Frequency analysis (Height VS Voltage)	49
Figure 7.7: Sensitivity analysis (Frequency VS Voltage)	50
Figure 7.8: Pressure VS Displacement Analysis (Rectangular shape of active size element):	51
Figure 7.9: Pressure VS Displacement Analysis (Circular shape of active size element):	52

LIST OF SYMBOLS, ABBREVIATIONS AND ACRONYMS

e_{nm}	Piezo-electric constants
g_{33}	Piezo Stress constant
d_{33}	Piezo Strain Constant
D_e	Electric displacement
E_e	Electric field
ε	Permittivity
V_{PVDF}	Voltage response of the PVDF film
E	Young's modulus
ϑ	Poisson's ratio
ρ	Mass Density
P	Sound pressure
c	Sound speed
k	Wave number
ω	Angular frequency
U	Mechanical displacement
D	Directivity response
S	Sensitivity of the PVDF hydrophone

CHAPTER 1: INTRODUCTION

1.1 BACKGROUND AND MOTIVATION

In the 21st century, underwater hydrophone acoustic sensing has gained significant attention due to its diverse applications. Acoustic waves are ideal for underwater communication because of their ability to travel long distances, making them the most effective medium for transmitting information in aquatic environments [1]. A key use of underwater acoustic sensing is identifying the direction and position of sound sources, including marine vessels and aquatic organisms. These functions are crucial for enhancing safety, improving transportation efficiency, and aiding in marine mammal conservation efforts [2].

Sound pressure, as a fundamental physical parameter, has been extensively studied and measured in underwater environments. Highly sensitive hydrophones are essential for accurate sound pressure detection, which is critical for various scientific and industrial applications [1]. Beyond sound pressure, other methods like acoustic vector sensing have emerged to provide more detailed data. These include measurements of acoustic particle velocity and acoustic intensity, offering insights beyond basic sound pressure readings [2]. Acoustic intensity, which combines sound pressure and particle motion, measures the power flow of a sound wave. It reveals the direction of energy flow and the rate of energy transport through a given area, aiding in the understanding of sound wave propagation [3].

Due to the critical need for accurate underwater acoustic measurements, substantial progress has been achieved in the development of hydrophones and acoustic vector sensors. Different applications require hydrophones with varying designs and sensing mechanisms. Most hydrophones globally are based on the piezoelectric effect, where specific materials produce an electric charge in response to mechanical stress. Polyvinylidene fluoride (PVDF) is one of the most

commonly used piezoelectric materials for underwater sensing due to its mechanical and piezoelectric properties, as well as its acoustic impedance, which closely matches that of water. Although PVDF is commonly employed for sound pressure measurement in the megahertz range, its sensitivity diminishes at lower frequencies, reducing its efficiency within this spectrum. Additionally, when used in vector sensors, controlling PVDF's directivity response is crucial for accurate measurements. Therefore, further research is necessary to enhance the sensitivity of PVDF hydrophones, especially for low-frequency applications.

Constructing a vector hydrophone typically follows one of two methods. One approach involves using two omni-directional pressure sensors spaced apart to estimate the pressure gradient. The second method focuses on creating a sensor that directly measures particle motion, providing more detailed information about the acoustic environment. Although PVDF is generally regarded as suitable for vector sensors, relatively little research has been conducted on its use in this area. The potential for PVDF-based vector sensors and intensity probes is still being explored, and further investigation is needed to fully realize its capabilities.

1.2 PERFORMANCE MATRICS

These performance metrics are essential for assessing the hydrophone's capability in detecting and analyzing underwater acoustic signals. Each metric provides insight into the hydrophone's operational efficiency and suitability for specific environmental conditions. Together, they help in optimizing the design and selection of hydrophones for different underwater applications[1]

Table 1.1: Comparison of Piezoelectric Properties

Property	units	PVDF	PZT (PZT 5A)
Density	10^3 kg/m^3	1.78	7.5
Relative Permittivity	$\frac{\epsilon}{\epsilon_0}$	12	1200
d33 Constant	10^{-12} C/N	33	374
g33 Constant	10^{-3} Vm/N	340	24
Acoustic Impedance	$10^6 \text{ kg/m}^2\text{-sec}$	2.7	30

1.2.1 Sensitivity

The sensitivity of a hydrophone refers to its capacity to transform acoustic pressure into an output voltage when exposed to quasi-planar acoustic pressure waves at normal incidence, with the response varying based on frequency. Since underwater acoustic signals are typically weak and non-contact, high sensitivity is crucial for ensuring optimal hydrophone performance [2]. When sensitivity remains consistent across the frequency band in the pressure spectrum, a simple scaling factor (S) can be applied for adjustment. However, for broadband signals, such as nonlinear ones containing multiple harmonics, sensitivity can vary significantly across the frequency range. In these cases, deconvolution provides a more accurate adjustment compared to basic scaling methods [1].

In underwater acoustics, hydrophone sensitivity is generally measured in decibels (dB, re: 1 V/Pa) rather than in the linear unit of mV/MPa, which is more commonly used at higher frequencies. For instance, a sensitivity of -240 dB (re: 1 V/Pa) corresponds to 1 V/MPa [3]. The sensitivity can be expressed mathematically as:

$$S=20\log\left(\frac{V}{P}\right) - 120 \quad (1.1)$$

where V represents the change in the hydrophone's output signal as a result of increased acoustic pressure P . A reference sensitivity level of 1 V/Pa is considered standard[2]. For multidimensional hydrophones, sensitivity is defined for each axis, and a balanced multi-axis sensitivity greatly simplifies signal processing [3].

1.2.2 Frequency Response (Bandwidth)

A temporally localized acoustic signal encompasses a wide range of frequencies, making it essential for hydrophones to precisely measure various acoustic frequencies. In other words, hydrophone sensitivity tends to be frequency-dependent, and understanding this relationship is crucial. One of the key factors limiting bandwidth is the hydrophone's resonance frequency, which significantly affects its overall performance. It is generally recommended to operate hydrophones below their resonance frequency to maintain a consistent transfer function across a broad frequency range. Consequently, hydrophones are often engineered with mechanical resonance frequencies that are several times higher than their intended operating range [6].

Additionally, fluid-structure interaction plays a crucial role in influencing the hydrophone's bandwidth. Zhang et al. [4], through the use of a Fluid-Structure Interaction (FSI) mathematical model, examined the effects of this interaction on resonance frequency and other performance parameters. Typically, a frequency range of 20 Hz to 1.5 kHz is adequate for detecting low-frequency underwater acoustic signals.

1.2.3 Directional Response (Directivity)

Hydrophones are generally classified into two primary categories based on their directivity: omni-directional and directional hydrophones. Omni-directional hydrophones detect acoustic waves with equal sensitivity from all directions, whereas directional hydrophones exhibit greater sensitivity to sound waves approaching from specific angles. The sensitivity of a hydrophone is also affected by the angle between its acoustic axis and the direction of the incoming sound wave [7]. Directional hydrophones, which are designed to capture sound primarily from certain directions, can be created either by combining multiple omni-directional units or by forming an array of hydrophones. In such arrays, the time differences in wave arrival at each sensor are used to determine the direction of the incoming acoustic signal.

1.2.4 ACTIVE SIZE ELEMENT

The size of the active element in a hydrophone is critical for several reasons. Firstly, when positioned in an actual acoustic field, the hydrophone should cause minimal disturbance to the original sound environment. However, in reality, hydrophones can introduce unwanted noise due to their presence, which may affect measurement accuracy, particularly in fast-flowing conditions [59]. According to acoustic theory, the scattering of incident acoustic waves by the hydrophone can be disregarded if the condition $ka \ll 1$ is satisfied, where k represents the acoustic wavenumber and a denotes the size of the hydrophone.

For underwater acoustic detection with working frequencies below 2000 Hz, the acoustic wavenumber k remains under 8.37, where $k=2\pi f/v$ and v is the velocity of sound in water (1500 m/s). When the pickup unit's size satisfies $ka \ll 1$, such as with an active element size of 1000 micrometers, minimal distortion in the sound field occurs. This condition allows the sound field to

remain undisturbed, making it ideal for low-frequency signal detection underwater. In your case, since the active element has a rectangular shape, similar principles apply to ensure minimal interference and accurate low-frequency monitoring.

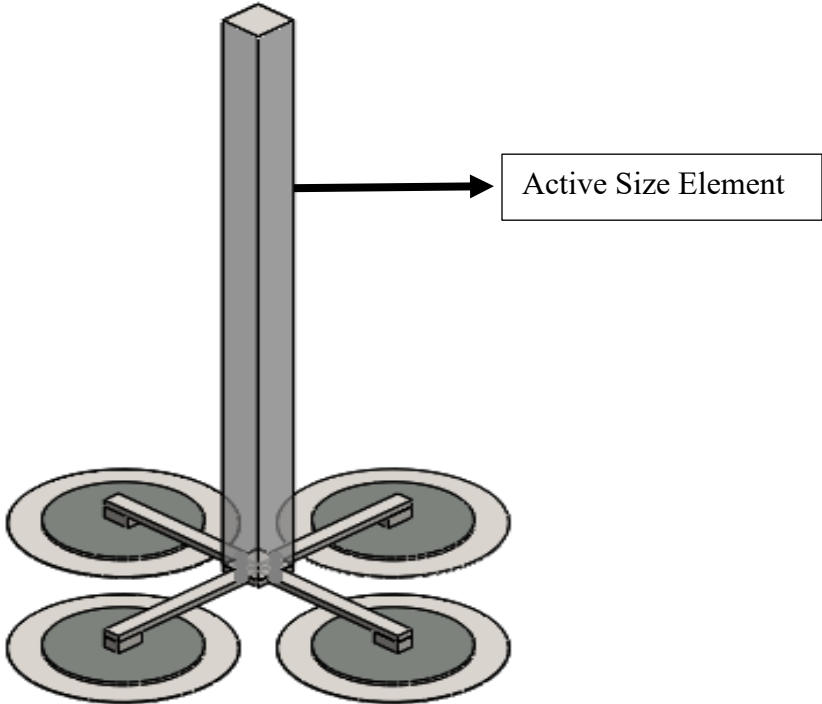


Figure 1.1: Active Size Element (Vertical Cilium)

1.2.5 Acoustic Impedance

One of the most important factors in hydrophone design is the acoustic impedance (Z), which measures how effectively energy is transferred between the hydrophone's active material and the surrounding medium. Acoustic impedance can be described as:

$$Z=\rho V \quad (1.2)$$

where ρ is the density of the material, and V is the speed of sound in the medium [130]. Acoustic impedance is expressed as the product of the radiation area, density, and sound speed. A close match between the acoustic impedance of the hydrophone's active element and the surrounding medium allows for more efficient transfer of incident energy, minimizing energy loss or reflection at the interface. This ensures that more energy is transmitted into the active element, thereby enhancing the hydrophone's response. Since water has an acoustic impedance of approximately 1.5 MRayl [131], piezoelectric materials with similar acoustic impedance values are ideal for underwater applications. Furthermore, the material used to encapsulate the hydrophone must also have an acoustic impedance close to that of water to maintain transparency at the operating frequencies, further enhancing the device's performance.

1.3 MEMS UNDERWATER HYDROPHONE

MEMS (Micro-Electro-Mechanical Systems) underwater hydrophones are highly sensitive acoustic sensors designed for detecting and recording underwater sounds. Unlike traditional hydrophones, which are typically bulkier and rely on piezoelectric materials, MEMS-based hydrophones offer several advantages, including miniaturization, lower power consumption, and cost efficiency. These devices are engineered to perform in challenging underwater environments, with features such as high sensitivity, wide frequency response, and good directional characteristics. MEMS hydrophones typically use capacitive or piezoresistive sensing elements to convert pressure variations in water into electrical signals[5]. Due to their small size, they can be deployed in large arrays for applications like underwater surveillance, oceanographic research, and environmental monitoring. Their compact form factor and scalability make MEMS hydrophones suitable for use

in autonomous underwater vehicles (AUVs) and other remote sensing platforms. Additionally, their integration with modern signal processing technologies allows for enhanced performance in detecting low-frequency sounds, such as those generated by marine life or underwater geological activities[6].

1.4 PROBLEM STATEMENT

In the development of underwater vector hydrophones, achieving high sensitivity while maintaining the desired bandwidth is a critical challenge. Traditional piezoelectric materials such as PZT (lead zirconate titanate) have been widely used in hydrophone applications, but their inherent limitations in terms of flexibility and sensitivity at lower frequencies restrict performance, particularly in the bandwidth of 20 Hz to 1.5 kHz. The problem addressed in this thesis involves replacing PZT with PVDF (polyvinylidene fluoride), a piezoelectric polymer known for its flexibility and better performance in low-frequency environments. The objective is to enhance the sensitivity of the MEMS-based PVDF underwater vector hydrophone, ensuring that it operates effectively within the specified frequency range while maintaining optimal signal integrity and durability in underwater conditions.

1.5 RESEARCH OBJECTIVES

Building on the insights from the literature review, the research objectives can be distinctly articulated as follows:

- To conduct an in-depth study of how PVDF film responds to underwater sound using simulations and numerical techniques.

- To investigate ways to adjust the design parameters of PVDF hydrophones in order to achieve improved sensitivity.

1.6 METHODOLOGY

The methodology for this research focuses on validating the performance of a MEMS-based PVDF underwater vector hydrophone through simulation and numerical analysis. The approach involves designing a detailed model of the hydrophone, followed by simulations to evaluate its sensitivity and frequency response across a bandwidth of 20 Hz to 1.5 kHz. Finite Element Method (FEM) analysis is used to study the hydrophone's structural behavior both with and without fluid-structure interaction (FSI). Results validation is conducted by comparing the simulated performance with existing theoretical models and literature data, ensuring accuracy and alignment with previous research. Through parametric analysis, key design parameters are optimized to achieve the best sensitivity results.

CHAPTER 2: LITERATURE REVIEW

2.1 Underwater Hydrophone

Hydrophones play a crucial role in recording underwater sound pressure data and have attracted considerable interest from researchers globally. Various hydrophone designs have been developed to cater to different application needs, with most being made from piezoelectric materials such as piezo-ceramics and piezo-polymers [1]. Piezo-ceramics are particularly well-suited for converting electrical signals into acoustic waves, making them an excellent choice for generating sound in underwater environments. In contrast, piezo-polymers excel as sensing materials due to their high sensitivity and broad frequency response, making them well-suited for broadband hydrophones [9]. Among these materials, polyvinylidene fluoride (PVDF) polymer stands out for its consistent, flat frequency response, high mechanical flexibility, and low acoustic impedance [10]. Moreover, PVDF's versatility allows it to be shaped for various hydrophone designs or applied to curved surfaces, making it an excellent choice for underwater sound measurement [10].

The frequency and directional response requirements for hydrophones largely depend on the specific application and measurement conditions. Therefore, understanding how factors such as materials, shape, and dimensions influence the hydrophone's performance is crucial. Numerous studies have explored these aspects. For example, [11] used a finite-element model to examine how geometric and material factors affect the sensitivity of a cylindrical piezo-ceramic hydrophone [12]. Additionally, LeBlanc (1978) provided handbooks on hydrophone element design to help engineers select the optimal combination of materials and geometry for specific needs [11]. However, as the

following section will discuss, further research is needed to enhance our understanding and control of PVDF hydrophones' performance. Beyond these factors, designing a high-performance hydrophone requires optimizing characteristics such as compact size, high signal-to-noise ratio, wide dynamic range, and excellent linearity. More information on these design considerations can be found in the review work [1].

2.2 Types of Hydrophones

Hydrophones are specialized instruments designed for detecting and measuring underwater sound. They come in different types, each suited to specific tasks and environments. Two broad categories of hydrophones exist, with distinct characteristics that make them valuable for various applications in marine research, underwater navigation, and acoustic monitoring.

The choice of hydrophone depends on the specific requirements of the application, as each type offers unique advantages. Understanding these differences is crucial for selecting the appropriate hydrophone to achieve optimal results in underwater acoustic studies.

2.2.1 SCALAR HYDROPHONE

Scalar hydrophones, also known as sound pressure hydrophones, are widely used in underwater sound measurements and are specifically designed to measure scalar quantities like sound pressure in the sound field [7]. They are particularly useful in applications where only the pressure variations of the sound waves need to be captured, such as in basic underwater acoustic monitoring or simple sonar systems. Scalar hydrophones work by detecting changes in the pressure of the sound waves, which allows for the measurement of sound pressure levels and frequencies, providing critical information about the underwater acoustic environment [8]. Due to their simplicity and effectiveness, scalar hydrophones are commonly used

in many underwater applications, from marine research to naval sonar systems [9]. However, while scalar hydrophones provide accurate pressure measurements, they do not capture vector information such as particle velocity, which limits their ability to fully represent the complexity of underwater sound fields. Nonetheless, scalar hydrophones are valued for their stability, ease of use, and reliable performance in sound pressure detection [10].

2.1.2 VECTOR HYDROPHONE

The development of vector hydrophones dates back to the 1940s, marked by the use of inertial sensors to directly measure the vibration velocity of water mass points. With rapid advancements in Micro-Electro-Mechanical Systems (MEMS), the field has evolved toward greater integration, miniaturization, and intelligence. Recently, researchers have designed a range of MEMS-based bionic structures to improve sensor performance. For example, Herzog et al. developed a flow sensor array modeled after the lateral line system [11], while Quattieri et al. created an AlN pressure-sensitive cantilever for artificial lateral line systems [12]. Bionic MEMS sensors have also been explored in vector hydrophones. Zhang et al. designed a 3D omni-vector piezoresistive hydrophone by mimicking the auditory mechanism of a fish's lateral line organ, integrating the bionic microstructure onto a chip using MEMS technology [13]. This hydrophone provides benefits such as compact size, enhanced consistency, and high sensitivity. Additionally, the mechanical flexibility and shape adaptability of PVDF film make it a promising material for use in bionic MEMS hydrophones.

2.3 UNDERWATER ACOUSTIC SENSORS

Acoustic vector sensors are extensively used to measure vector quantities such as the acoustic pressure gradient, acceleration, and particle velocity at specific points within an acoustic field. Unlike traditional pressure hydrophones, these sensors provide more detailed insights by detecting the direction of acoustic waves [16]. This ability makes them particularly valuable for applications like source localization and target identification. Recent technological advances have made it possible to measure acoustic particle velocity or acceleration using neutrally buoyant inertial sensors, generating significant interest in the field. Several cutting-edge designs have been developed, including the cilia-type four-beam vector hydrophone [17], the T-shape vector hydrophone, and the thickness-shear-mode vector hydrophone. Beam-type structures with fixed boundary conditions are especially favored for their compact size and reliable sensing performance. These beams respond to the motion of fluid particles generated by acoustic waves, aiding in determining the direction of sound propagation. Additionally, cantilever-type acoustic vector piezoelectric sensors have been designed, offering exceptionally high sensitivity, typically ranging between -190 dB and -160 dB [16].

2.4 PVDF Polymer

Since Kawai's discovery of PVDF's piezoelectric properties in 1969, extensive research has been conducted to investigate its use in sensors and actuators [16]. PVDF is particularly suitable for these applications due to its excellent mechanical and piezoelectric properties. It has found widespread use in areas such as force transduction, vibration monitoring, structural health assessment, and portable medical diagnostics [17]. When compared to lead zirconate titanate (PZT), a widely used piezoelectric ceramic, PVDF boasts a piezoelectric voltage constant that is roughly 20 times higher and an acoustic impedance match with water that is 10 times more favorable, making it an ideal material for underwater acoustic sensors.

PVDF is a semi-crystalline polymer that can exist in multiple crystalline states, with its degree of crystallinity having a significant effect on its piezoelectric constant. Like most piezoelectric polymers, PVDF contains crystalline regions with internal dipole moments. Before polarization, these dipoles are randomly oriented, resulting in a net dipole moment of zero. However, processes such as mechanical stretching and electrical poling under a strong electric field can align the crystalline regions, significantly enhancing the piezoelectric constant of the bulk PVDF film and making it more effective for sensing applications [18]. Additionally, the polarization process imparts anisotropic properties to the material, meaning that PVDF exhibits different responses depending on the direction of applied forces.

Various types of PVDF films with differing properties and sensitivities are available on the market, with Measurement Specialties being one of the most widely used suppliers. The parameters used in this thesis are based on PVDF films obtained from this company.

Table 2.1: Material Analysis of PVDF Disc

$E(\text{N/m}^2)$	ν	ρ (kg/m ³)	Pressure wave $c(\text{m/s})$	g_{31} (Vm/N)	g_{32} (Vm/N)	g_{33} (Vm/N)
1.8×10^9	0.42	1780	1606.7	0.209	0.0418	≈ 0.3
ν_r	d_{31} (C/N)	d_{32} (C/N)	d_{33} (C/N)	e_{31} (C/m ²)	e_{32} (C/m ²)	e_{33} (C/m ²)
108×10^{-12}	23×10^{-11} ₂	4.6×10^{-12}	33×10^{-11} ₂	0.01	≈ 0.013	≈ 0.06

2.5 PVDF Disc as An Underwater Acoustic Sensor

PVDF film exhibits a relatively high hydrostatic response compared to other piezoelectric materials, such as PZT ceramics, primarily due to its larger piezoelectric voltage constant. Its minimal disruption to the sound field during measurements also makes it highly suitable for

underwater acoustic applications. Consequently, numerous researchers have explored the use of PVDF in hydrophone development. PVDF hydrophones have been successfully applied in ultrasonic fields and are often used for the calibration of ultrasound devices [4]. Various PVDF-based hydrophone designs, including membrane-type and needle-type, have been created for frequencies extending into the megahertz range, gaining considerable popularity. For instance, a miniature PVDF-based needle hydrophone was designed for ultrasonic field measurements, while a membrane hydrophone was developed with a bandwidth of up to 150 MHz.

Although PVDF hydrophones developed for low-frequency applications have been documented, they are relatively rare. For instance, membrane-type hydrophones with larger diameters were created to provide adequate sensitivity, but these membranes are susceptible to rupturing under hydrostatic pressure, even in shallow water. To mitigate this issue, various designs have been introduced that incorporate elastic structures to reinforce the PVDF film. Examples include flexural disk hydrophones and composite cylinder hydrophones made with PVDF, which have achieved sensitivity levels of -200 dB and -212 dB, respectively. In 1985, Moffett et al. proposed a hydrophone design that matched the impedance to water, resulting in a smooth frequency response between 5 kHz and 1000 kHz, with a sensitivity of -190 dB using a 20.5 dB pre-amplifier. Later developments, such as the use of thicker PVDF film, allowed a cylindrical hydrophone to reach a sensitivity of around -190 dB. Despite these improvements in performance, the fabrication process remains complex and expensive, limiting the practicality of these designs due to the need for large film sizes and intricate assembly methods.

To address these challenges, simpler methods to increase PVDF sensitivity have been investigated. It has been found that laminating PVDF between thin stiff plates can enhance its sensitivity . Additionally, experimental results suggest that attaching PVDF films to elastic materials can

modify their response, further enhancing performance . This thesis explores the idea of using different coating materials to control the response of PVDF films.

On the other hand, while PVDF has shown potential for use as an acoustic vector sensor and intensity probe, limited research has been conducted in this area. designed a cantilevered PVDF bimorph hydrophone, demonstrating that its output is proportional to the incident particle velocity normal to the surface, suggesting its use in acoustic intensity measurements with a single sensor . More recently, Killeen et al. (2009) developed prototype intensity probes using parallel PVDF films based on the P-P method, where the pressure-related outputs of the PVDF were used to estimate pressure and pressure gradient components . Although these developments demonstrate the potential of PVDF for intensity probes, further research is needed before such sensors can be reliably constructed and used for precise measurements.

CHAPTER 3: WORKING PRINCIPLE OF HYDROPHONE

The working principle of a hydrophone is inspired by the **bionic principle of the fish lateral line**. Like how fish use their lateral line system to detect minute vibrations and changes in water pressure, hydrophones are designed to sense underwater acoustic signals. This bio-inspired design allows for efficient detection of sound waves, making hydrophones an essential tool in underwater research and communication.

3.1 Cilia-Type Four-Beam Vector Hydrophone

In the design of the new sensor structure, a beam configuration is used as the cilia, while piezoelectric materials function as the neuromasts. This fish-inspired design includes two key components: (1) a power transmission section consisting of a beam and four anchors, and (2) the sensor structure, which contains two electrodes with piezoelectric material positioned between them. When sound pressure impacts the beam, it is concentrated on the top electrode of the piezoelectric sensor through the anchors, causing the diaphragm to bend. This bending induces stress and strain within the diaphragms, corresponding to the applied sound pressure [14]. As a result, the piezoelectric material becomes polarized, creating a potential difference between its two ends. This generated potential is then transmitted to the output via the electrodes, allowing the sound to be measured. The sensor structure is designed to detect sound waves on a plane perpendicular to the beam (x, y plane) [15].

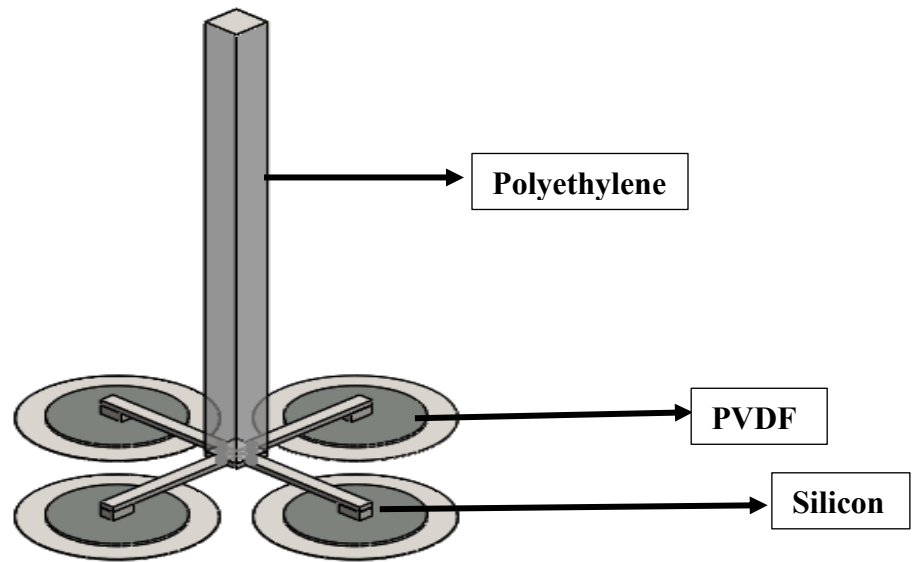


Figure 3.1: Cilia Four Beam Vector Hydrophone

Table 3.1: Material Properties of the Material

Material	Density (kg/m³)	Young's Modulus (GPa)	Poisson's Ratio
Polyethylene	950	.2	.42
Silicon	2330	130	.28
PVDF	1780	4	.35

In this configuration, the beam is connected to four piezoelectric diaphragms. When sound waves impact the beam, it bends in the direction of the incoming sound, creating stress and strain in the attached diaphragms. This force results in the polarization of the piezoelectric material within the diaphragms, allowing the detection of sound direction[15]. The initial step in designing this sensor involves developing a mathematical model of the structure to predict its behavior and performance.

3.1.1 Bionic Principle of The Sensor

Fish and aquatic amphibians possess a natural lateral line organ, a specialized sensory system that enables them to detect variations in water pressure [16]. This mechanosensory system extends from the head to the tail of the fish and is made up of individual neuromasts, each containing hundreds of hair cells. As illustrated in Fig. 1, the hair cells consist of bundles of mechanoreceptor structures (stereocilia) and a single kinocilium, which extends from the apical side of the cells. The hair cells are encased in a gelatinous sensory cupula, which serves as a protective barrier between the external water environment and the kinocilium. The hair cells are connected to nerves that link to the medulla oblongata via the lateralis nerve. The schematic drawing of fish lateral line as shown in **fig 3.2**[13]

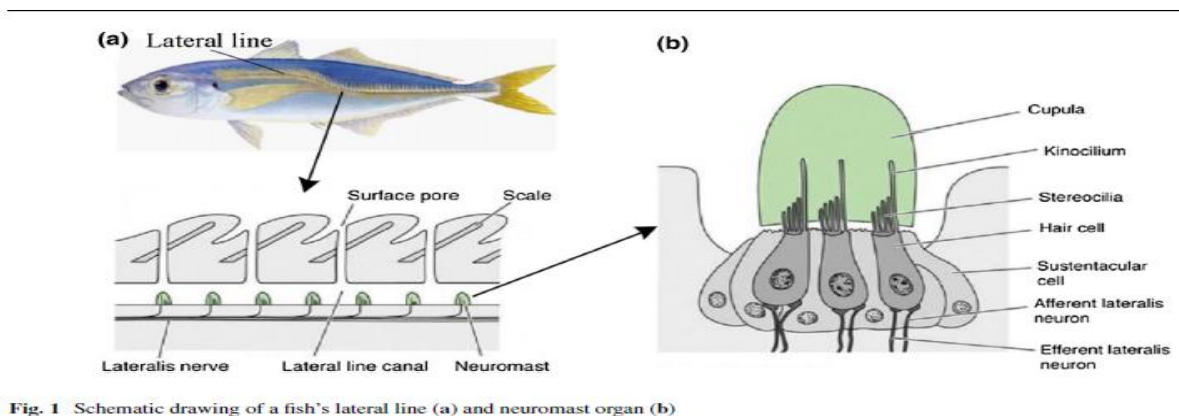


Figure 3.2: (a) Schematic drawing of fish lateral line (b) neuromast organ

When external forces such as sound waves, vibrations, or changes in water flow velocity create turbulence, this disturbance enters the lateral line canal system of the fish through small surface pores. The resulting pressure exerts force on the mucus, which flows toward the neuromasts and causes the sensory cupula to move. This movement, in turn, deflects the hair bundle (comprising stereocilia and kinocilium) via the lymphatic fluid inside the cupula. The kinocilium, which extends

from the apical side of the cell, transmits this mechanical stimulus to the hair cells. The motion within the hair cells propagates through synapses to the nerve fibers at the base of the hair cells, stimulating the sensory cells. These signals are then transmitted to the medulla oblongata through the sensory nerve fibers and the lateral nerve [17], [18]. **Fig.3.3**[13] depicts the sequence of sense transmission within the fish's acoustic o-lateralis system.

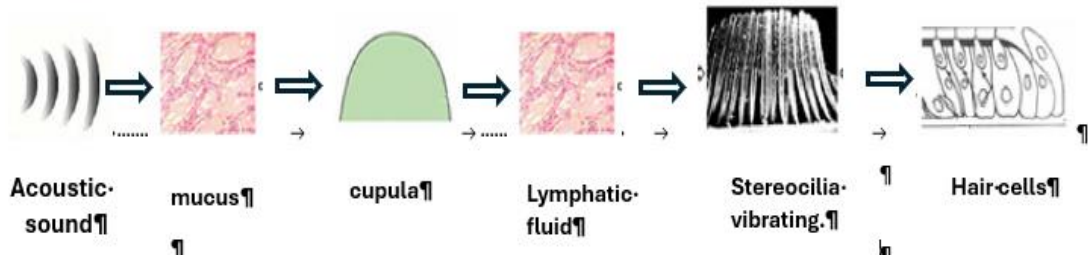


Figure 3.3: Sense-conducting pathway of a fish's lateral line organ

The density of the fish's cupula is nearly identical to that of the surrounding water, allowing it to move with the same amplitude as the water particles. Numerous experimental studies have demonstrated that the lateral line system of fish is highly sensitive to low-frequency fluid motions that are parallel to the lateral line. The key features of this sensory mechanoreceptor system include the ability to detect the orientation and direction of incoming sound waves, as well as the perception of water movement and low-frequency sound waves.

3.2 Direction Detector Model of Acoustic Wave

3.2.1 Direction Detection Principle

Using a plane wave as an example, the acoustic state at any point in space can be characterized by pressure, medium density, and vibration velocity expressed as $p(r, t)$, $\rho(r, t)$, $v(r, t)$, respectively, which are the functions of both time and space. According to the acoustic principle, the relationship between the vibration velocity and sound pressure can be expressed as (1-3).

$$P(r, t) = P_0 e^{j(\omega t - \vec{k} \cdot \vec{r})} = P_0 \exp\{i(\omega t - kx \cos \alpha \cos \theta - ky \cos \alpha \sin \theta - kz \sin \alpha)\} \quad (3.1)$$

Where P_0 is the hydrostatic pressure, K is the acoustic wave vector describing the direction propagation of sound wave, θ (azimuth angle) is the angle between the horizontal projection of the wave vector and the X axis, range of the azimuth angle is $[0, 2\pi]$, α (elevation angle) is the angle between the wave vector (k) and the horizontal plane, range of elevation angle is $[-\frac{\pi}{2}, \frac{\pi}{2}]$, ω is the angular velocity of the acoustic signal ($k = \frac{\omega}{c}$) where c is the speed of sound in water, t represent the time and r represent the point and the sound source[19]. As shown in figure.

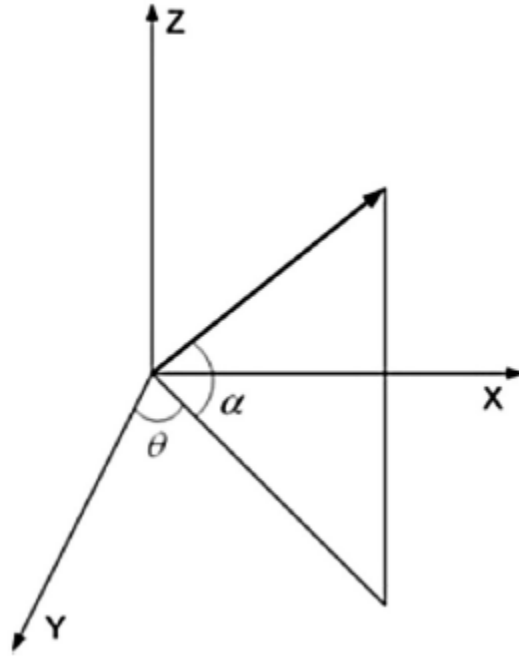


Figure 3.4: The projection in the rectangular coordinate system of the wave vector

According to acoustic theory, the change in momentum (velocity) of particles is related to the pressure gradient of a sound field in a homogeneous medium is

$$\frac{dv(r,t)}{dt} + \frac{1}{\rho} \nabla p(r,t) = 0 \quad (3.2)$$

$v(r, t)$ and $p(r, t)$ is the Particle velocity and sound pressure as a function of position and time respectively, ρ is the medium density and ∇ is the gradient operator[20].

$$\vartheta(r,t) = -\frac{1}{\rho} \int \nabla p(r,t) dt \quad (3.3)$$

$$\vartheta(r,t) = -\frac{1}{\rho} \iint \nabla [X(\omega) e^{j(\omega t - kr)}] d\omega dt \quad (3.4)$$

$$\vartheta(r,t) = -\frac{p(r,t)}{\rho c} (\cos \theta \cos \alpha \hat{x} + \sin \theta \cos \alpha \hat{y} + \sin \alpha \hat{z}) \quad (3.5)$$

Where $\hat{x}, \hat{y}, \hat{z}$ are the unit vectors of the X, Y and Z-axis, respectively and ρc represent the acoustic impedance of sound waves. The difference between sound pressure and particle velocity components is simply a constant, and their waveforms are identical. In other words, for plane waves, they are perfectly correlated, meaning the particle velocity can be used to fully represent the sound field[21]

It can be seen from the Eq. (3.2), for plane waves, the particle velocity can be used to describe the sound field. The three particle velocity components are obtained from Eq. (3.6-3.8):

$$v_x = \frac{p}{\rho c} \cos \theta \cos \alpha \quad (3.6)$$

$$v_y = \frac{p}{\rho c} \sin \theta \cos \alpha \quad (3.7)$$

$$v_z = \frac{p}{\rho c} \sin \alpha \quad (3.8)$$

Therefore

$$\theta = \arctan \left(\frac{V_x}{V_y} \right) \quad (3.9)$$

$$\alpha = \arctan \left(\frac{V_z}{\sqrt{V_x^2 + V_y^2}} \right) \quad (3.10)$$

Thus, by measuring the two particle velocity components V_x and V_y , in the horizontal plane, we can determine the azimuth angle θ of the sound source using Equation (3.9). Additionally, the three velocity components allow us to calculate the pitch angle α using Equation (3.10). These are the fundamental principles that a vector hydrophone employs to locate the position of a sound source.

CHAPTER 4: SENSING MECHANISM OF A PVDF HYDROPHONE

It is essential to understand how a polyvinylidene fluoride (PVDF) film responds to sound to develop effective PVDF hydrophones. This involves examining the connection between the film's sensitivity and the sound waves it encounters. When a plain PVDF film is directly exposed to a sound field, pressure is applied to its boundaries, leading to the buildup of stress within the film. As a result of the piezoelectric effect, an electric potential difference forms between the film's two surfaces, which the electrodes pick up as a voltage signal. Therefore, the primary focus is on analyzing how the film reacts to stress from the incoming sound waves.

4.1 Piezoelectric Effect and Its Constitutive Equations

Piezoelectricity is the ability of specific materials to produce an electrical charge when they experience mechanical pressure or, conversely, to transform electrical energy into mechanical movement or strain. This unique property was discovered by the Curie brothers back in 1880. The word "piezoelectricity" comes from the Greek term "piezo," which means "to press." Over the years, piezoelectric materials have been extensively used in sensors and actuators, particularly for larger-scale applications, and more recently, they've gained prominence in MEMS (Micro-Electro-Mechanical Systems) technology.

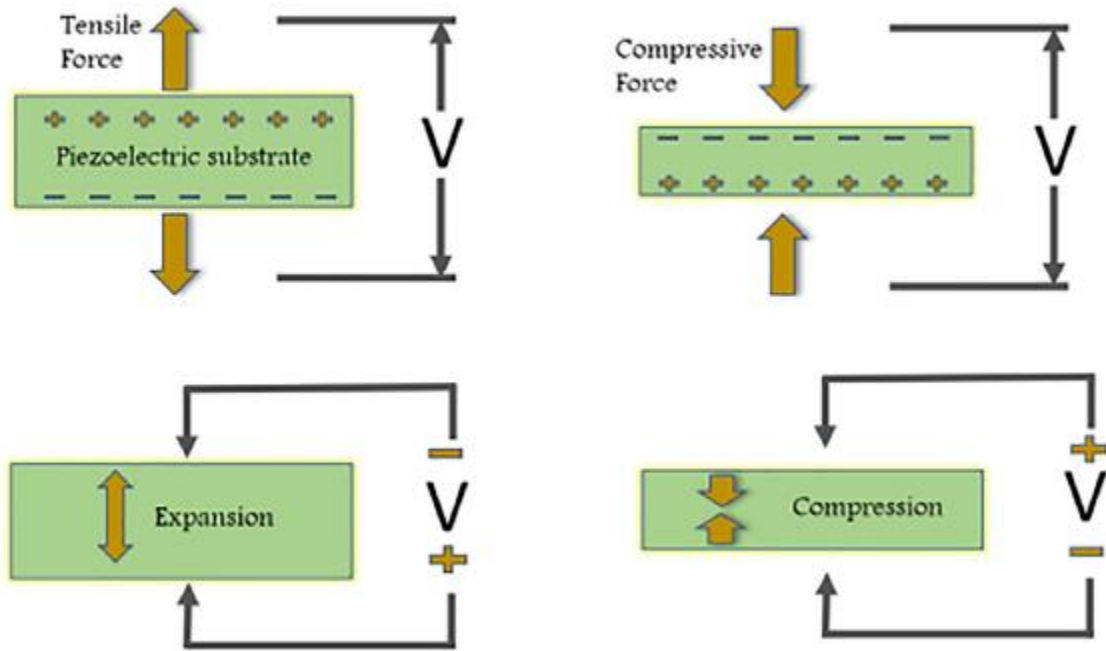


Figure 4.1: Schematic drawing of the (a) direct, (b) converse piezoelectric effect

Figure 4.1 provides a schematic representation of the core principles behind piezoelectricity and its application in both sensing and actuation. Commonly used piezoelectric materials include lead zirconate titanate (PZT), quartz, zinc oxide, and polyvinylidene difluoride (PVDF). These materials tend to be brittle, requiring careful handling during packaging to avoid damage. Instead of being used independently, piezoelectric materials are typically integrated with flexible structures to enhance their sensing and actuation functions. Due to their sensitivity to high temperatures, they are not suitable for extreme thermal environments. Piezoelectric actuators can produce significant displacements, and piezoelectric sensors are regarded as self-powered since they generate a voltage in response to applied mechanical stress.

4.1.1 Constitutive Equations for The Sensing Mode

The constitutive equations for the sensing mode capture how piezoelectric materials respond to mechanical stress by generating electrical charge or polarization. In this mode, piezoelectric

materials convert mechanical energy, such as stress or strain, into electrical energy, which is represented by electrical displacement or polarization. These relationships can be expressed mathematically through the constitutive equations, which describe the material's behavior under mechanical and electrical influences. For the sensing mode, the equation can be written as:

$$\{D\}_{3 \times 1} = [d]_{3 \times 6} \{T\}_{6 \times 1} + [\epsilon]_{3 \times 3} \{E\}_{3 \times 1} \quad (4.1)$$

- $\{D\}_{3 \times 1}$ is the vector of electrical displacements or polarization (charge per unit area), with units of Coulombs per square meter (C/m²). This vector represents the electrical response of the piezoelectric material.
- $[d]_{3 \times 6}$ the piezoelectric coefficient matrix, which describes the relationship between mechanical stress and the resulting electrical displacement. The elements of this matrix have units of Coulombs per Newton (C/N).
- $\{T\}_{6 \times 1}$ is the mechanical stress vector (with six components: three normal and three shear), with units of Newtons per square meter (N/m²).
- $[\epsilon]_{3 \times 3}$ is the permittivity (dielectric constant) matrix, which describes the material's ability to store electrical energy in the presence of an electric field. The elements of this matrix have units of Farads per meter (F/m) or Coulombs per Voltmeter (C/Vm).
- $\{E\}_{3 \times 1}$ is the applied electric field vector (with three orthogonal components: x, y, and z or 1, 2, and 3), measured in Volts per meter (V/m)[23].

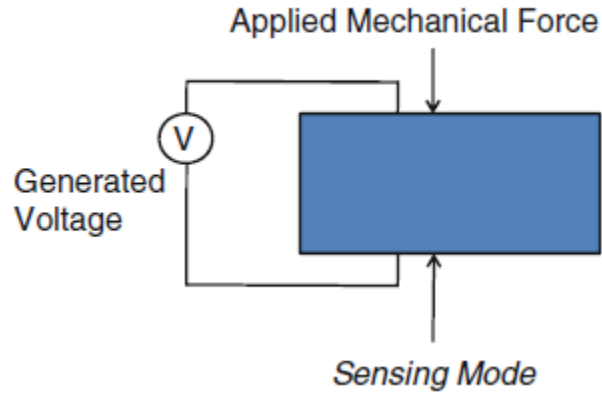


Figure 4.2: Piezoelectricity in both sensing mode

In this equation, the term $[d]_{3 \times 6} \{T\}_{6 \times 1}$ represents the generation of electric displacement due to mechanical stress, while the term $[\epsilon]_{3 \times 3} \{E\}_{3 \times 1}$ accounts for the electrical response due to an applied electric field. This equation captures the coupling between mechanical and electrical phenomena in piezoelectric materials, where mechanical stress results in electrical displacement, making it useful for sensing applications.

4.1.2 Constitutive Equations for The Actuation Mode

The constitutive equations for the actuation mode describe the behavior of piezoelectric materials when subjected to an electric field, causing mechanical deformation (stress or strain). In the actuation mode, piezoelectric materials convert electrical energy into mechanical energy, which is characterized by mechanical strain and stress.[24], [25]. The constitutive equation for the actuation mode can be expressed as:

$$\{S\}_{6 \times 1} = [s]_{6 \times 6} \{T\}_{6 \times 1} + [d]_{6 \times 3} \{E\}_{3 \times 1} \quad (4.2)$$

In this context, $\{S\}$ and $\{T\}$ represent the material's mechanical strain and stress vectors, respectively, with three normal components and three shear components. The matrix $[s]$ is the compliance matrix, which is the inverse of the stiffness matrix, while $[d]$ contain the piezoelectric constants. $\{E\}$ represents the applied electric field vector along the x, y, and z (or 1, 2, and 3) directions. The units are: T in Newtons per square meter (N/m^2), S in square meters per Newton (m^2/N), d in Coulombs per Newton (C/N), and E in Volts per meter (V/m).

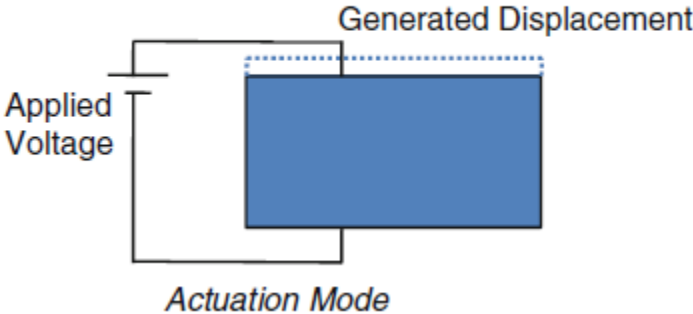


Figure 4.3: Piezoelectricity in both actuation mode

CHAPTER 5: HYDROPHONE OPERATING MECHANISM

Most piezoelectric hydrophones are currently designed to operate within a broad frequency range below their resonant frequency, which ensures a flat frequency response. However, recent research has suggested that operating hydrophones closer to their resonant frequency may offer advantages, particularly in improving sensitivity for detecting weak signals and studying nonlinear emissions from gas-filled bubbles. This approach has also shown potential in medical fields, such as vibro-acousto-graphy, a novel ultrasonic imaging technique. Traditionally, the hydrostatic model has been employed to analyze piezoelectric hydrophones at off-resonant frequencies, but its limitations become evident near the resonant frequency due to the abrupt changes in electromechanical behavior. To overcome these challenges, a dynamic fluid-structure interaction model has been introduced, enabling a more accurate characterization of hydrophones over a wider frequency range, thus broadening their applicability across various domains.

5.1 Operating at the Resonance Frequency

The resonance frequency plays a pivotal role in determining a hydrophone's overall performance, especially regarding its bandwidth and sensitivity. Operating at or below the resonance frequency allows a hydrophone to measure acoustic signals across a wide range of frequencies with consistent accuracy. A high bandwidth is especially advantageous, as it enables the hydrophone to maintain a flat response below its resonance frequency, assuming electrical loading effects are minimal. This flat response means that the hydrophone can detect and measure acoustic signals over a broad frequency range without requiring complex calibration, which is particularly useful in applications like underwater sound detection or sonar systems.

High bandwidth hydrophones also offer improved resolution. Higher frequency acoustic waves have shorter wavelengths, allowing hydrophones with wide frequency capabilities to resolve

smaller objects or finer details in the acoustic field. This makes them ideal for precision applications where detecting subtle changes or small-scale features in the sound field is critical.

The resonance frequency is one of the most significant factors limiting a hydrophone's bandwidth, serving as a key indicator of performance. Operating below the resonance frequency reduces distortion and variations in sensitivity across different frequencies, resulting in a stable and accurate response. Below this point, the transfer function remains flat, allowing the hydrophone to perform uniformly across the desired frequency range.

It is generally recommended to design hydrophones so that their resonance frequency is significantly higher than the upper limit of the desired operating frequency band. This ensures the hydrophone stays well within its flat response range, avoiding the nonlinearities and peak sensitivities associated with operating near or at resonance, which can distort acoustic measurements.

Although most piezoelectric hydrophones are designed to function well below their resonance frequency to ensure a flat response over a wide bandwidth, recent studies indicate that operating near the resonance frequency can significantly enhance sensitivity in certain applications, such as weak signal detection or analyzing nonlinear emissions from gas-filled bubbles. For example, research has shown that hydrophones functioning closer to their resonance frequency could be beneficial in vibro-acoustography, a novel ultrasonic imaging technique for medical diagnostics.

Several models, including the hydrostatic model, finite element method (FEM), and electrical loading correction methods, have been developed to analyze piezoelectric hydrophones. The hydrostatic model is commonly used to describe and optimize hydrophone performance in off-resonant conditions. However, because this model is frequency-independent, it falls short when analyzing hydrophone behavior near resonance, where dynamic interactions dominate, and electromechanical responses vary quickly with changes in frequency. To address this limitation, a

dynamic fluid-structure interaction model has recently been introduced, enabling more comprehensive characterization of piezoelectric hydrophones over a broader frequency range.

5.2 Hydrophones Operation for Low-Frequency Applications

Low-frequency acoustic waves, typically below 10 kHz, are well-suited for underwater applications due to their beneficial properties, such as the ability to travel long distances, low interference, and strong penetration capabilities. These features make them ideal for various purposes, including disaster early warning systems (like earthquake and volcanic eruption detection), underwater target positioning, and military operations. Most low-frequency underwater hydrophones operate at frequencies below 500 kHz, and there is increasing interest in developing hydrophones for low-frequency applications, as lowering the acoustic field frequency does not significantly affect acoustic resolution.

In general, low-frequency non-optical hydrophones are larger in size, which improves sensitivity but also increases weight and output impedance. This, in turn, lowers the cut-off frequency, enhances the signal-to-noise ratio (SNR), improves directivity, and makes the hydrophone more sensitive to acceleration. However, the larger size also complicates depth control and handling hydrostatic pressure. As shown in Figure X, low-frequency hydrophones can easily achieve sensitivities between -220 dB and -200 dB. Encapsulating these hydrophones with polyurethane rubber can cause attenuation that worsens with increasing frequency, leading to a sharper decline in sensitivity beyond the resonant frequency.

Moreover, since low-frequency hydrophones generally lack preamplifiers or impedance buffers that could introduce noise, their noise equivalent power (NEP) is typically determined by the hydrophone's sensitivity and the noise floor of the data acquisition (DAQ) system. Similarly, the maximum pressure that a hydrophone can measure is governed not by the dynamic range of a preamplifier but by its

sensitivity and the maximum signal capacity of the DAQ system. In oceanic environments, it is rare to encounter acoustic signals exceeding 1 MPa or dropping below 100 kPa.

5.3 Mathematical modeling of piezoelectric sensor

According to the new structure characteristics, the establishment of new mathematical model will consist of two parts (1) power transmission section, includes cantilever beam and vertical cilia, (2) the sensitivity section, includes two electrode and the piezo polymer PVDF material between them. The shape of the sensitive structure of piezo polymer diaphragm would be circular. For a circular diaphragm with the fixed edge which the force of action in its central part. The mechanical sensitivity of a circular diaphragm is defined as (5.1):

$$S_m = \frac{dw}{dP} \quad (5.1)$$

The response is linear, when the clamped circular diaphragm experienced the small deflection (less than the 30% of its thickness), the displacement in z direction is given as (5.2)

$$w_z = \frac{PR^4}{64D} \quad (5.2)$$

where w, R and P are the deflection in z direction, radial distance and the pressure applied on the center of the diaphragm respectively. the flexural rigidity of the material is given as (5.3).

$$D = \frac{Et^3}{12(1-\nu^2)} \quad (5.3)$$

Where E, ν and t are the elasticity of modulus, poison ratio and the thickness of the diaphragm respectively. The homogenous pressure of the circular diaphragm of pvdf sensitive material with fixed edges can be calculated as (5.4):

$$P = \frac{64Dw}{R^4} = \frac{64Et^3 \times w}{12(1-\nu^2)R^4} \quad (5.4)$$

The mechanical sensitivity of the circular diaphragm can be obtained as:

$$S_m = \frac{dw}{dP} = \frac{R^2}{\pi t [5.33Et^2 / \pi R^2 (1-\nu^2)]} \quad (5.5)$$

The process of developing the combined mathematical model for power transmission involving the sensitive section of the hydrophone begins when a 10 Pa pressure is applied to the cilium, and the hydrophone is exposed to sound waves traveling along the x-axis. The resulting stress equation is formulated to account for the combined effects of the vertical cilia bending, which induces stress on the cantilever beams, while simultaneously causing deflection in the circular diaphragm. This deflection leads to stress in diaphragm A and strain in diaphragm B occurring simultaneously. The stress equation is represented as follows:

$$\sigma_{-x} = -\frac{(3PabH(H+t)(l^2+3dl))}{4ct^2+(2+\varepsilon)l^2+6bl} \pm K \times \omega_{-z} \quad (5.6)$$

Where a is the length of the vertical cilium, b is the width of the cilium and H is the height of the vertical cilium, $\varepsilon = 1/(1 + \mu)$, μ is the poison ratio of silicon, c is the width of the cantilever beam, and l is the length of the cantilever beam and d is the half length of the supporting block (2).

To develop the mathematical model for determining the natural frequency and frequency bandwidth of the vector hydrophone, the design must ensure that the resonance frequency of the structure is higher than the desired operational bandwidth. The natural frequency, which depends on the mechanical properties and structure of the hydrophone, can be expressed with the following formula:

$$f_1 = \frac{1}{2\pi} \sqrt{\frac{K_1}{m_{1H\alpha_1}}} \quad (5.7)$$

$$K_1 = \frac{2E_b ct^3}{3l^3} [(2+\varepsilon)l^2+6dl] + \frac{16E_{pvd} f t^3}{3R^4(1-\nu^2)} \quad (5.8)$$

$$K_2 = 3.0903 \cdot \frac{E_c I_c}{H^3} \quad (5.9)$$

$$I_c = \frac{a^2 b^2}{12} \quad (5.10)$$

$$m_1 = \rho a b H \quad (5.11)$$

$$\alpha_1 = \left(\frac{1}{8\lambda H} + \frac{m_{eq}}{2m_{1H}} \right) + \sqrt{\left(\frac{1}{8\lambda H} + \frac{m_{eq}}{2m_{1H}} \right)^2 - \left(\frac{m_{eq}}{4\lambda m_{1H}^2} - \frac{1}{\lambda 1.875} \right)} \quad (5.12)$$

$$m_{eq} = \rho_1 \frac{a b H^3}{3} + \rho_2 \left(\frac{1 a^2 b^2 h}{12} + \frac{1}{3} a b h^3 \right) \quad (5.13)$$

$$\lambda = \frac{k_2}{k_1} \quad (5.14)$$

Where E_b is the young modulus of the cantilever beam, E_c is the young modulus of the vertical cilium, I_c is the moment of inertia of vertical cilium, ρ_1 is the density of cilium and ρ_2 is the density of the silicon, m_1 and m_2 is the mass of the cilium and the mass of the center block respectively.

CHAPTER 6: FEM ANALYSIS OF UNDERWATER HYDROPHONE

The finite element method (FEM) analysis is a powerful tool for evaluating the performance of underwater hydrophones, particularly in understanding the interaction between mechanical and electrical properties in complex environments. In this analysis, both fluid-structure interaction (FSI) and non-FSI conditions are considered to assess the behavior of a cilia-based MEMS vector hydrophone. This hydrophone design incorporates cantilever beams attached to a supporting block, with the active sensing element made from polyethylene. The use of polyethylene is critical for density matching, as its density is like that of water, which is essential for maintaining the accurate vector measurement of the hydrophone.

Polyvinylidene fluoride (PVDF) is utilized as the primary sensing material in hydrophones because of its favorable acoustic impedance, which closely matches that of water. This property enables efficient transmission and reception of sound waves, making PVDF ideal for underwater applications. Additionally, its piezoelectric characteristics allow it to generate electrical signals in response to mechanical stress, enhancing its effectiveness as a sensing material in acoustic environments. This impedance matching ensures efficient energy transfer and enhances the hydrophone's sensitivity to underwater acoustic signals. Silicon is used for both the supporting block and the cantilever beams, providing the necessary mechanical support while maintaining the structural integrity of the hydrophone.

For the analysis without fluid-structure interaction (FSI), a piezoelectric Multiphysics simulation is employed to evaluate the hydrophone's performance in terms of mechanical stress and electric displacement generated within the PVDF sensing material. This approach helps in understanding

the pure piezoelectric response of the hydrophone without considering the surrounding fluid's influence.

In contrast, the analysis with FSI integrates both piezoelectric effects and acoustic-structure boundary interactions, which is crucial for accurately simulating the underwater environment where the hydrophone operates. This combined approach uses nonlinear analysis, which takes into account the complexities of fluid interaction with the hydrophone structure. The tolerance for accuracy in the FSI simulation is set to a high level, with a tolerance value of 0.001, ensuring precise results.

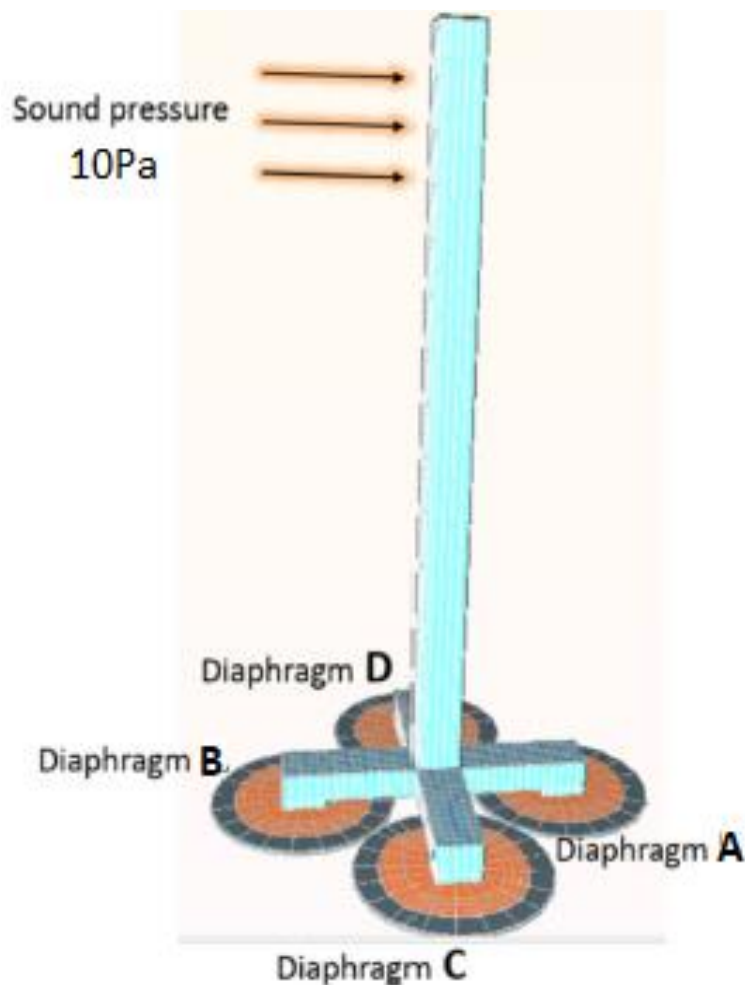


Figure 6.1: Vector hydrophone structure

The inclusion of FSI in the FEM analysis is essential for capturing the dynamic behavior of the hydrophone in real underwater conditions. It provides a comprehensive view of how sound waves interact with the structure and how the resulting mechanical vibrations influence the piezoelectric response. This dual approach—evaluating both with and without FSI—offers a holistic understanding of the hydrophone's operational efficiency and highlights areas for optimization in design and material selection.

6.1 Structural Analysis without FSI

In the first study of the structural analysis without fluid-structure interaction (FSI), a 10 Pa pressure is applied along the x-axis from Diaphragm B. The response of the system reveals a symmetrical behavior between Diaphragms A and B, which is a key observation in understanding the hydrophone's performance under applied mechanical stress.

When this pressure is applied, Diaphragm A undergoes compression, while Diaphragm B experiences tension. This opposing mechanical behavior results in both diaphragms generating voltages that are equal in magnitude but opposite in polarity. The piezoelectric material in the diaphragms, such as PVDF, is responsible for converting the mechanical stress into electrical output, and the polarity of the generated voltage is directly influenced by whether the diaphragm is under compression or tension. Diaphragm A, being compressed, produces a positive voltage, while Diaphragm B, under tension, produces an equal magnitude of negative voltage. This equal but opposite voltage generation demonstrates the balanced nature of the structure's response to applied stress.

Table 6.1: Non FSI Voltage and Displacement Response

Diaphragm	Voltage(V)	Displacement(um)

A	-9.05E-04	-6.47E-03
B	9.26E-04	6.55E-03
C	-5.90E-06	-2.57E-05
D	-4.81E-06	-4.71E-05

Additionally, the displacement and stress values in Diaphragms A and B are also symmetrical, reflecting the inverse relationship between compression and tension. Diaphragm A experiences inward displacement due to the compressive force, while Diaphragm B experiences outward displacement because of the tensile force. The stress distribution follows the same pattern, with compressive stress in Diaphragm A and tensile stress in Diaphragm B. This response is critical for ensuring the hydrophone's reliability in measuring underwater sound waves, as the symmetrical stress and displacement allow for accurate and stable readings from both diaphragms.

The eigenfrequency analysis of the hydrophone structure reveals important insights into its dynamic behavior. The mode shape analysis shows how the structure vibrates at specific frequencies, and in this case, the maximum amplitude is observed at 2 kHz. This resonance frequency is critical because it represents the point at which the structure exhibits the highest vibration amplitude when subjected to an external force or pressure.

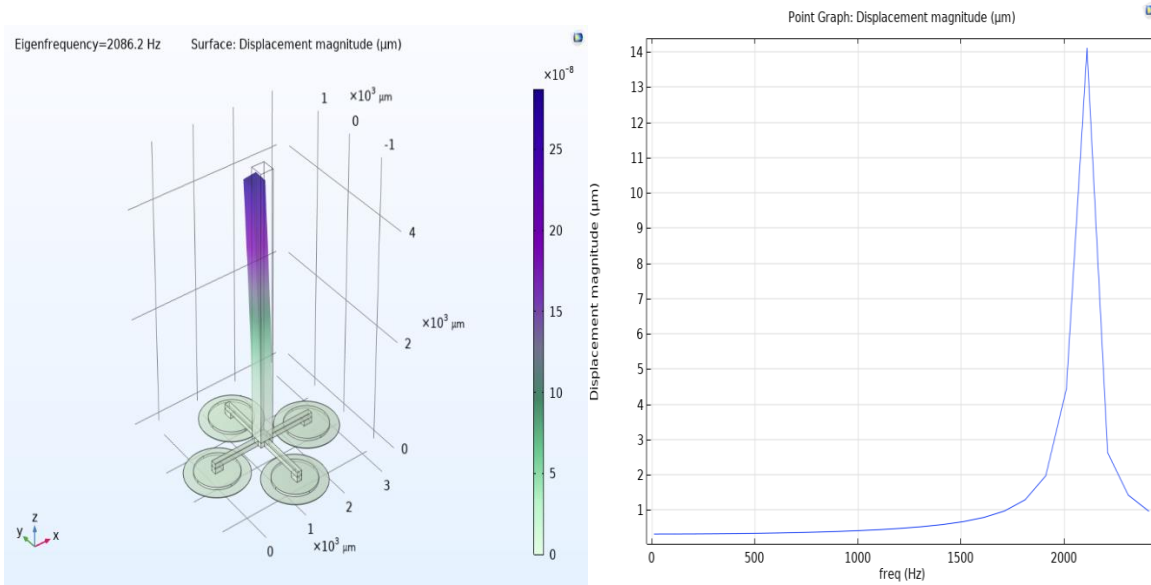


Figure 6.2: Modal analysis of vector hydrophone structure

At the eigenfrequency of 2 kHz, the hydrophone is most responsive to external stimuli, making it a crucial operational frequency for optimizing the device's sensitivity to acoustic signals. The maximum amplitude at this frequency indicates that the hydrophone's mechanical components, such as the diaphragms and the supporting block, experience the greatest displacement at this resonance point. Understanding this behavior is essential for fine-tuning the hydrophone design, as operating close to the resonance frequency can significantly enhance its performance, particularly in detecting weak or low-amplitude underwater acoustic signals.

6.2 Structural Analysis with FSI

In the structural analysis of the hydrophone with Fluid-Structure Interaction (FSI), several notable changes are observed compared to the non-FSI analysis. One of the most significant effects is the reduction in voltage, displacement, and stresses. This reduction is primarily due to the added mass and damping properties introduced by the surrounding water. When the hydrophone is submerged

in water, the fluid adds inertia and dissipates energy, leading to a decreased overall response of the sensor when subjected to the same applied pressure as in the non-FSI analysis.

The FSI analysis involves the coupling between the solid mechanics of the hydrophone structure and the surrounding fluid (water). In this case, the multiphysics environment is used, with pressure acoustic physics in the frequency domain accounting for the interaction between the solid hydrophone and the water medium. The presence of water influences the system by contributing mass and damping effects, which alters the dynamics of the structure.

Table 6.2: FSI Voltage and Displacement Response

Diaphragm	Voltage(V)	Displacement(um)
A	-7.64E-04	-5.14E-03
B	7.64E-04	5.14E-03
C	-2.84E-05	-1.65E-04
D	-2.15E-05	-1.79E-04

The water's added mass increases the inertia of the hydrophone, requiring more energy to produce the same level of motion as in the non-FSI case. This increased inertia dampens the vibrational response of the hydrophone to the applied pressure. As a result, the displacement of the hydrophone decreases in comparison to the structural analysis without FSI. Similarly, the stresses generated

within the structure are also reduced, as the system becomes less responsive to external forces due to the energy dissipation through the surrounding water.

Another key observation from the FSI analysis is the shift in eigenfrequency. In the non-FSI case, the eigenfrequency was observed at 2 kHz. However, when accounting for the effects of water in the FSI analysis, the eigenfrequency decreases to approximately 1.5 kHz. This shift is caused by the additional mass and damping effects introduced by the water, which slow down the system's vibrational response, leading to a lower resonant frequency.

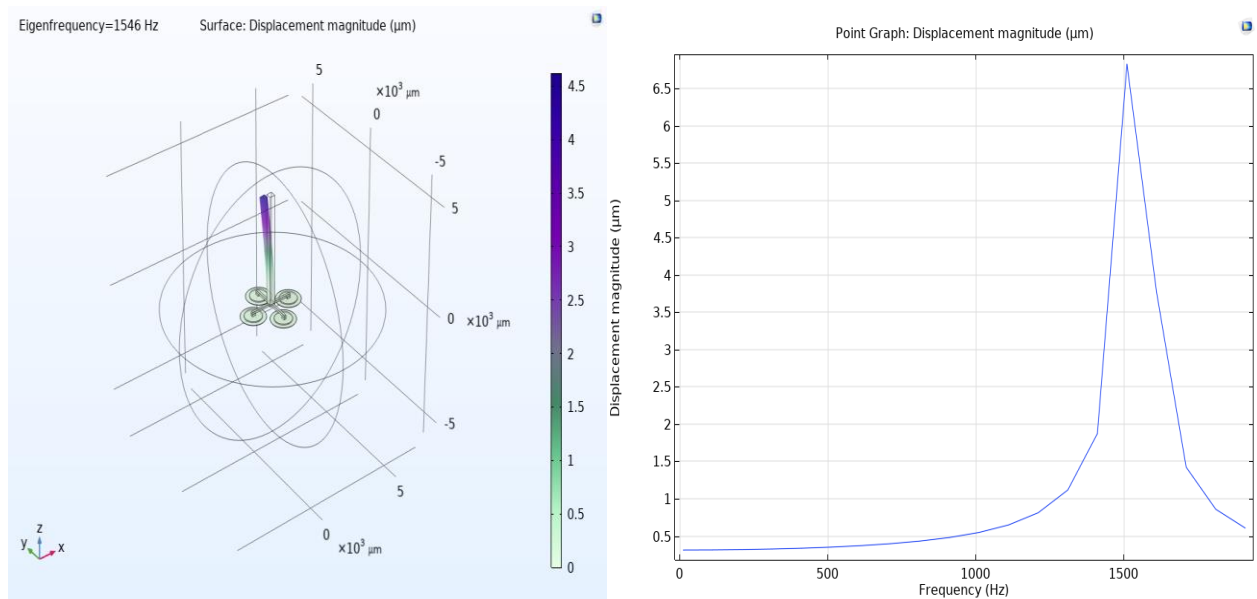


Figure 6.3: Wet (FSI) modal analysis of vector hydrophone structure

The mode shapes and frequency response graph also reflect this change. The frequency vs. displacement graph indicates a clear reduction in displacement amplitude at lower frequencies in the presence of FSI. This analysis highlights the critical impact of water on the performance of the hydrophone and the importance of considering FSI when designing sensors for underwater applications.

By incorporating FSI, the analysis provides a more realistic understanding of how the hydrophone behaves in its actual operational environment. It allows designers to account for the reduced

sensitivity and altered frequency response, ensuring that the hydrophone can still meet performance requirements despite the dampening effects of the water.

CHAPTER 7 RESULTS AND DISCUSSIONS

7.1 Parametric Scans of Design Parameters

In the design and optimization of PVDF-based underwater hydrophones, achieving optimal sensor sensitivity is crucial for practical applications. To address this, I performed a series of parametric scans on key design parameters, each with a significant impact on the overall performance of the hydrophone. These parameters include the thickness of the beam, the height of cilium, the thickness of the PVDF circular disc, and the pressure versus voltage response based on the shape of the active size element.

Through the four simulations, I systematically explored the influence of these parameters on sensor sensitivity. By adjusting each parameter, I was able to identify the optimal configuration that enhances sensitivity while maintaining stability and reliability under underwater conditions. These simulations provided clear insights into the design considerations necessary for practical use, with detailed explanations and results to follow.

For each design parameter, I will now present the simulation results, discussing their impact on the hydrophone's performance and justifying the selection of the most efficient configurations.

7.1.1 Thickness of the Cantilever Beam

7.1.1.1 Stationary Analysis

The first graph demonstrates the relationship between the thickness of the beam and terminal voltage. As the thickness increases, the generated voltage shows a rising trend. This indicates that greater beam thickness results in enhanced voltage generation, highlighting the correlation between the beam's structural integrity and its ability to generate a measurable voltage.

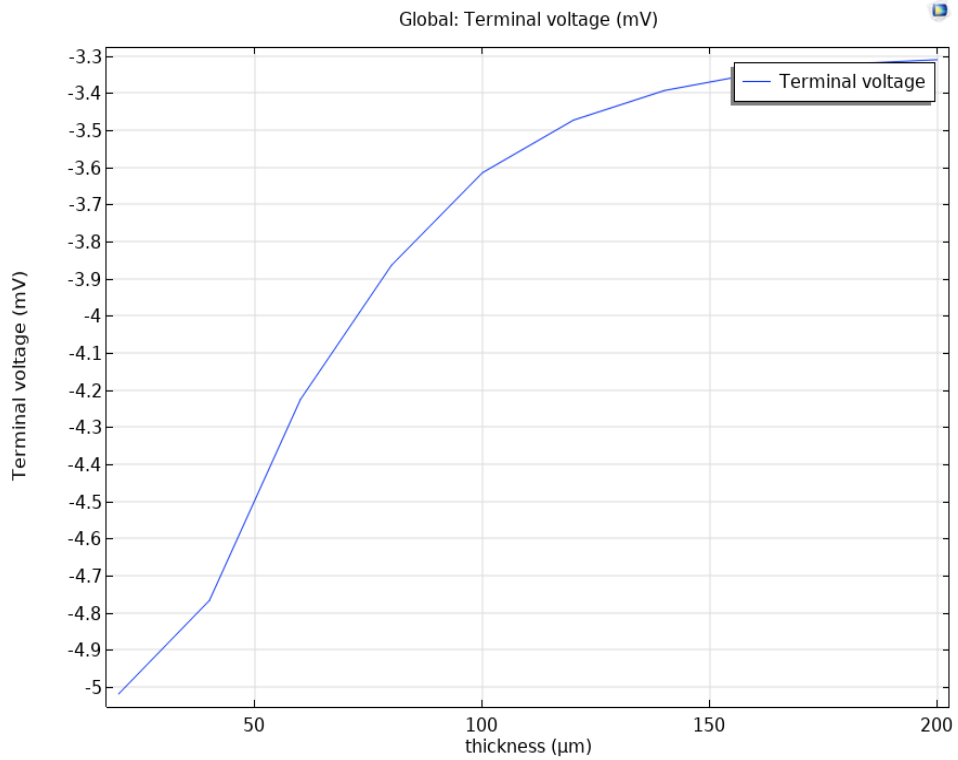


Figure 7.1: Stationary analysis (Thickness VS Voltage)

7.1.1.2 Modal Analysis

This step involved a modal analysis of the PVDF cantilever beam under Fluid-Structure Interaction (FSI). The second graph shows how the eigenfrequency of the cantilever increases with thickness. As the beam thickens, the natural frequency rises, leading to better dynamic performance in underwater environments, where eigenfrequencies can play a critical role in vibration behavior and structural stability.

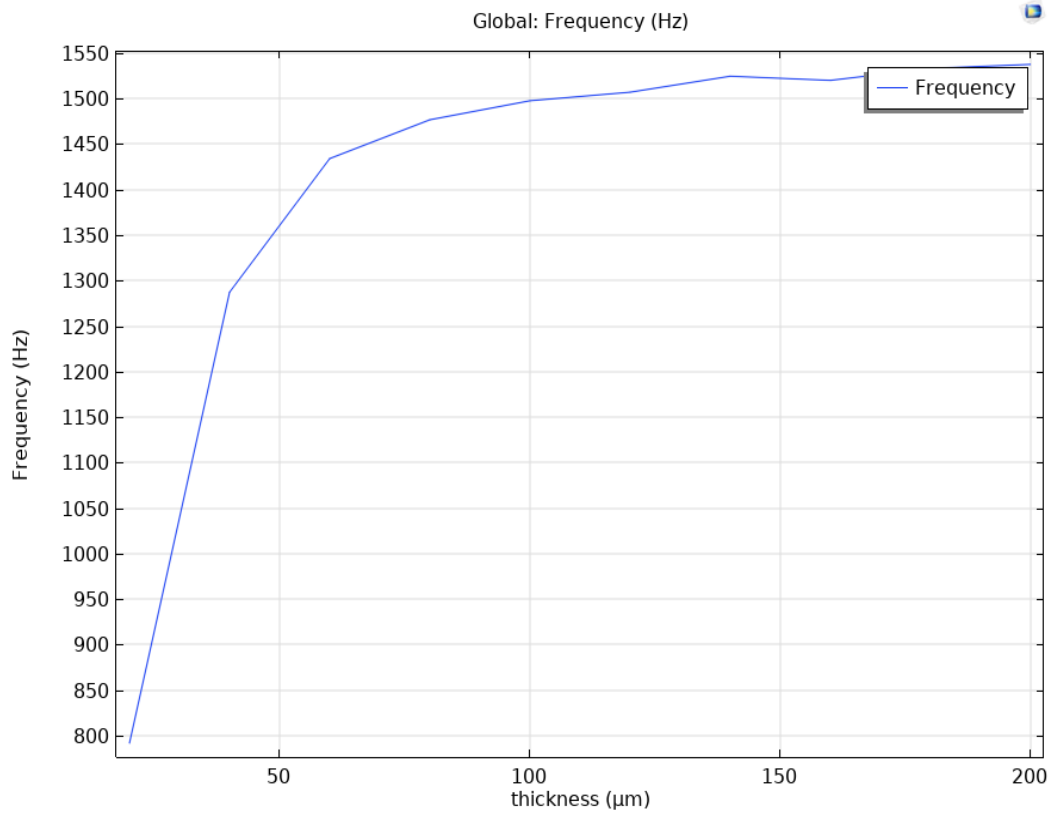


Figure 7.2: Modal Analysis (Thickness VS Frequency)

7.1.1.3 Sensitivity Analysis

In this analysis, the sensitivity of the beam was studied as a function of thickness, ranging from 20 μm to 200 μm. Based on the graph of frequency vs. sensitivity, it was observed that a thickness of 60 μm provides the optimal balance, delivering the best sensitivity performance across the frequency range. This makes the 60 μm beam thickness ideal for practical applications where both sensitivity and dynamic performance are critical.

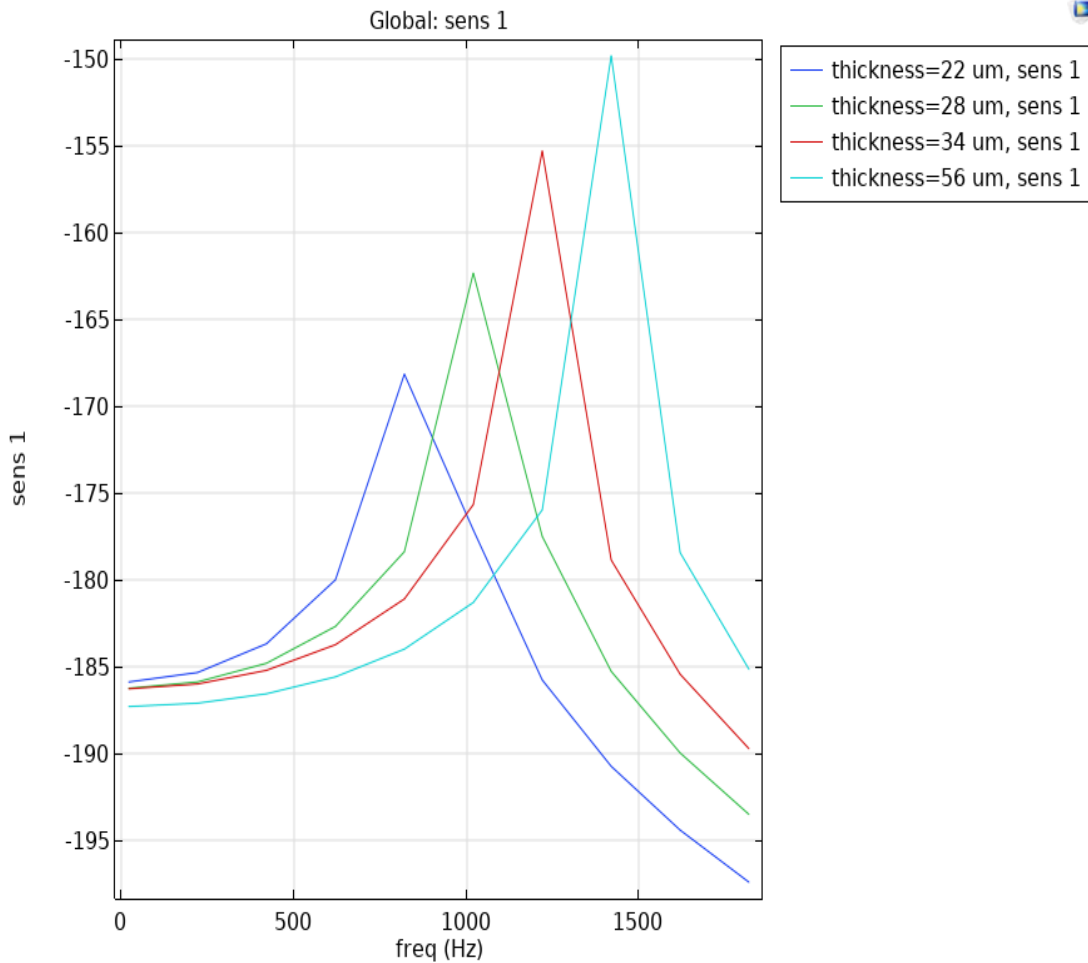


Figure 7.3: Sensitivity Analysis (Frequency VS Sensitivity)

7.1.2 Height of the Vertical Cilium

For the parametric scan of the height of the vertical cilium, I performed four analyses to examine how this design parameter affects the hydrophone’s performance:

7.1.2.1 Stationary Analysis:

The first graph illustrates the relationship between cilium height and terminal voltage. As the height of the vertical cilium increases (ranging from 2500 μm to 5000 μm), the generated voltage also rises. This indicates that taller cilia enhance the ability of the sensor to

generate higher voltages under static conditions, likely due to increased surface area interacting with pressure changes in the fluid environment.

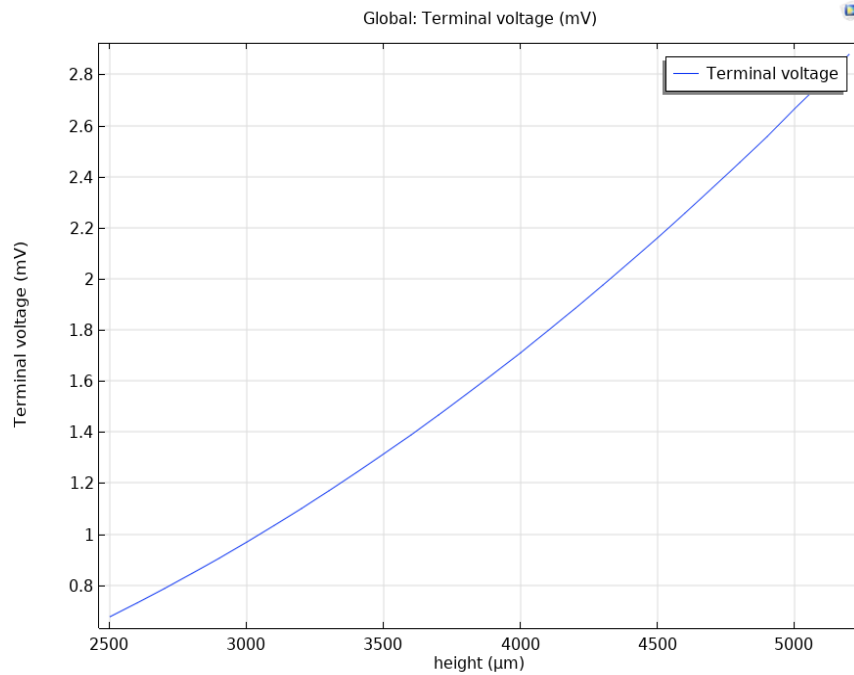


Figure 7.4: Stationary analysis (Height VS Voltage)

7.1.2.2 Modal Analysis:

The second analysis is a modal analysis, focusing on the eigenfrequency of the PVDF cantilever beam under (FSI). In this case, eigenfrequency of cantilever decreases with increasing cilium height. This is due to the added mass from the taller cilium, which shifts the natural frequency lower. While this reduces the beam's dynamic frequency range, the increase in height still yields a voltage gain, albeit at the cost of reduced eigenfrequency.

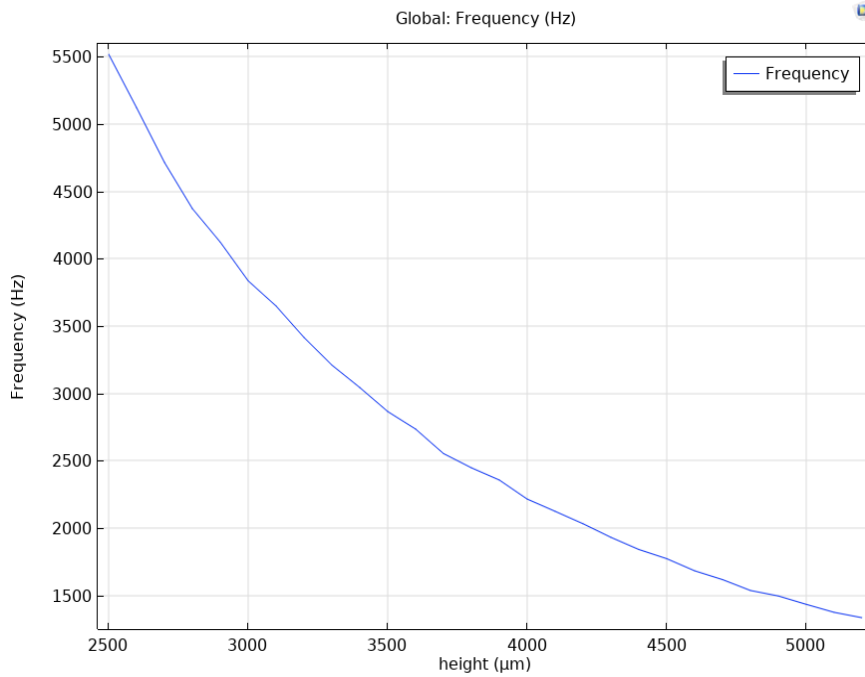


Figure 7.5: Modal analysis (Height VS Freq)

7.1.2.3 Frequency Analysis:

In this frequency analysis, I examined how the cilium height affects the beam's response across the operational bandwidth of 20 Hz to 1.5 kHz. Similar to the stationary analysis, voltage output continues to rise as frequency increases, maintaining the same trend as height increases. The graph shows voltage vs. cilium height at 50 Hz, but this trend persists across the entire frequency range up to 1.5 kHz, with voltage output improving with increasing cilium height.

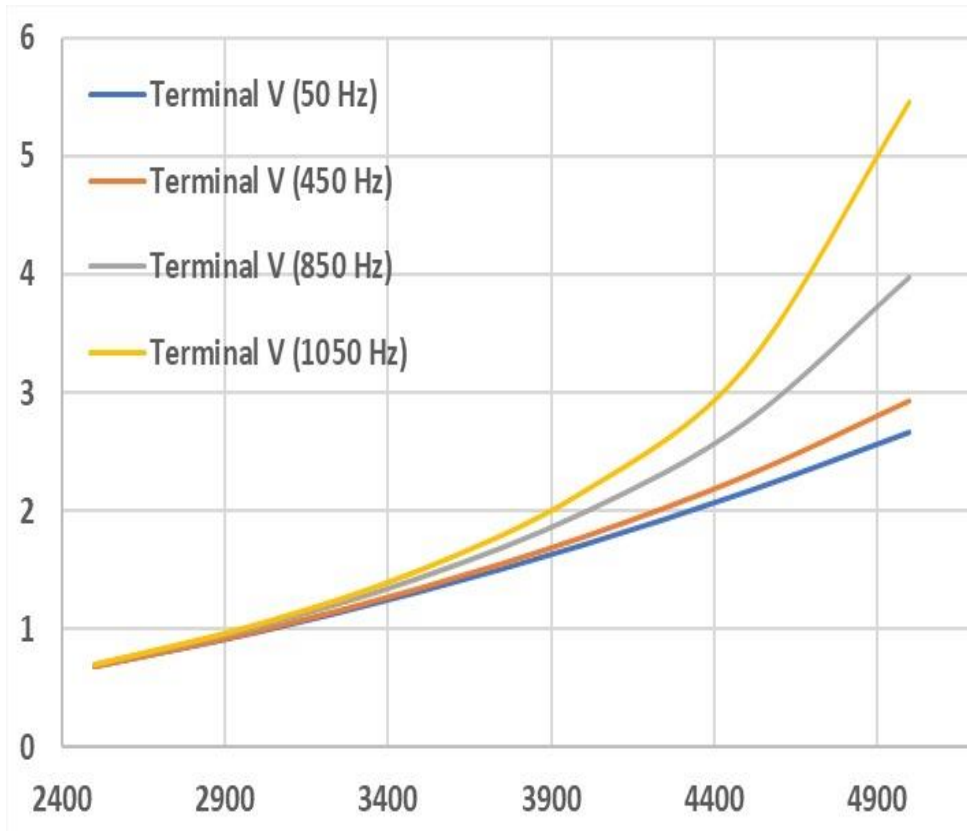


Figure 7.6: Frequency analysis (Height VS Voltage)

7.1.2.4 Sensitivity Analysis:

The sensitivity of the vertical cilium was analyzed as a function of height. Based on the graph plotting frequency vs. sensitivity, it was observed that increasing the height from 2500 μm to 5000 μm improves the sensor's sensitivity, with the 5000 μm height providing the best performance. This suggests that while increased height lowers the natural frequency, the overall sensor sensitivity is enhanced, making 5000 μm the ideal height for optimal sensitivity in practical applications.

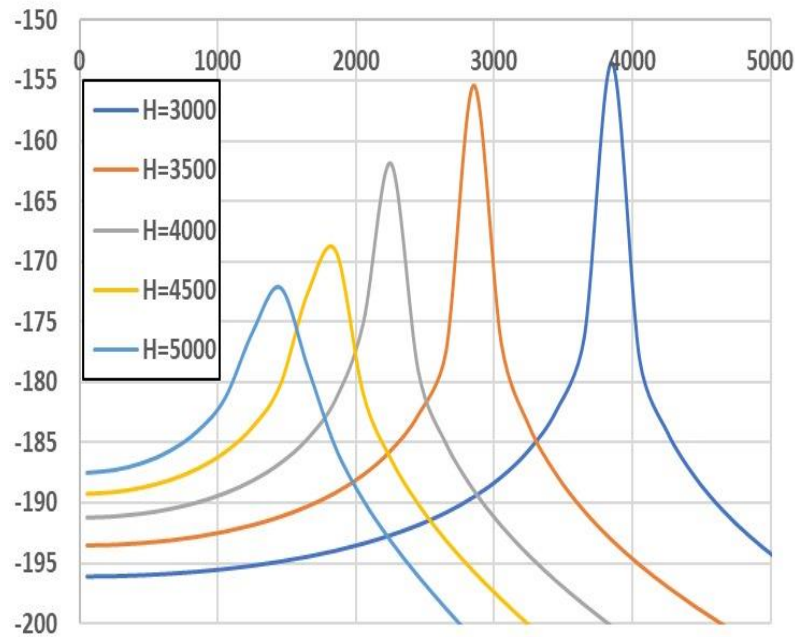


Figure 7.7: Sensitivity analysis (Frequency VS Voltage)

7.1.3 Pressure VS Displacement Analysis (shape of active size element)

The analysis reveals that the shape of the vertical cilium has a significant impact on the displacement experienced by the structure under varying pressure conditions. The parametric sweep was performed with pressure ranging from 0.01 Pa to 500 Pa, and it was observed that more displacement occurs when the vertical cilium is rectangular compared to when it is circular.

7.1.3.1 Rectangular Shape

The maximum displacement for the rectangular cilium shape was recorded at 0.045 μm . The rectangular shape contributes to more significant displacement due to its larger surface area, which allows it to interact with a greater amount of fluid. This increased interaction amplifies the force exerted by the fluid pressure, leading to higher structural deformation. Additionally, the rectangular cilium's geometry provides more flexural capacity, making it more responsive to applied forces and resulting in greater displacement. The larger surface area helps distribute pressure more evenly, facilitating enhanced movement.

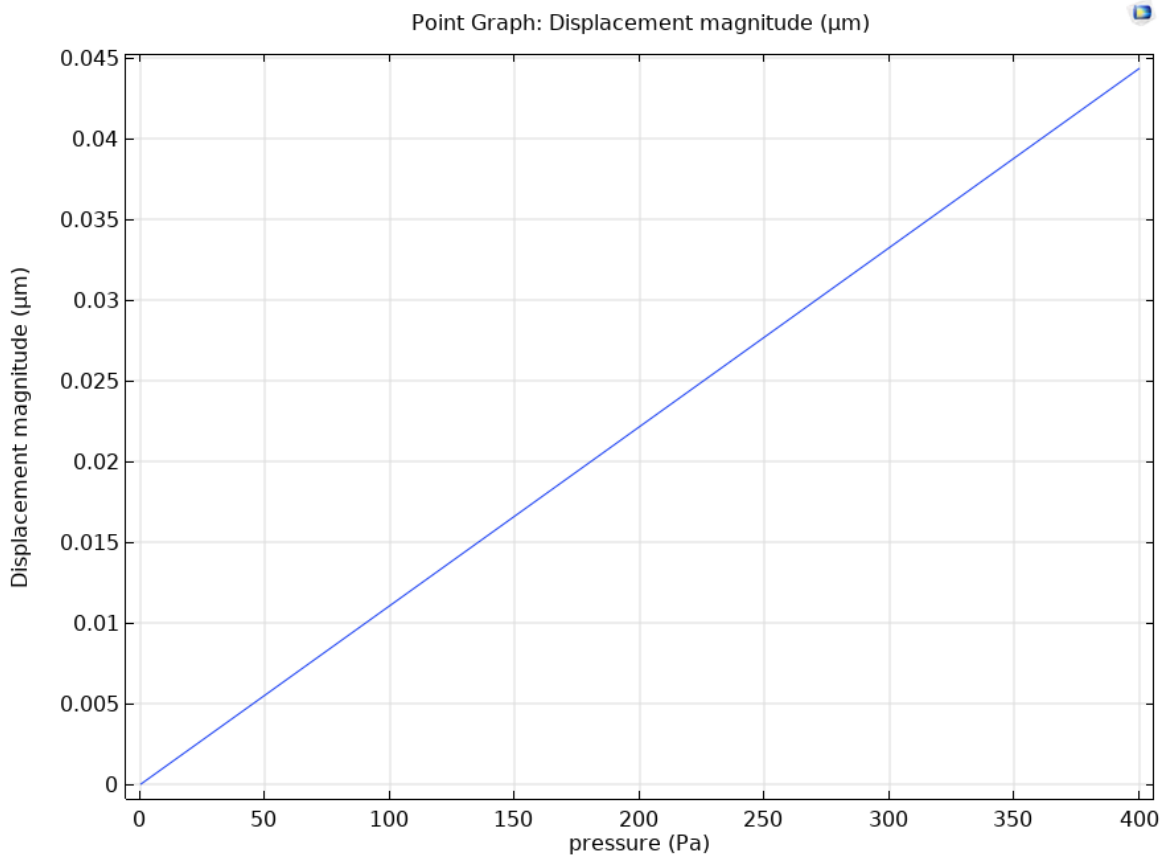


Figure 7.8: Pressure VS Displacement Analysis (Rectangular shape of active size element)

7.1.3.2 Circular Shape

For the circular cilium shape, the maximum displacement was lower, at 0.036 µm. The circular geometry inherently has less surface area compared to the rectangular shape, meaning it covers less fluid and therefore experiences lower forces from pressure interaction. While the circular shape may provide better uniformity in stress distribution, it is less effective in creating large deformations due to its smaller interaction surface. As a result, the displacement is lower, reflecting the circular shape's reduced capacity to flex under applied pressure.

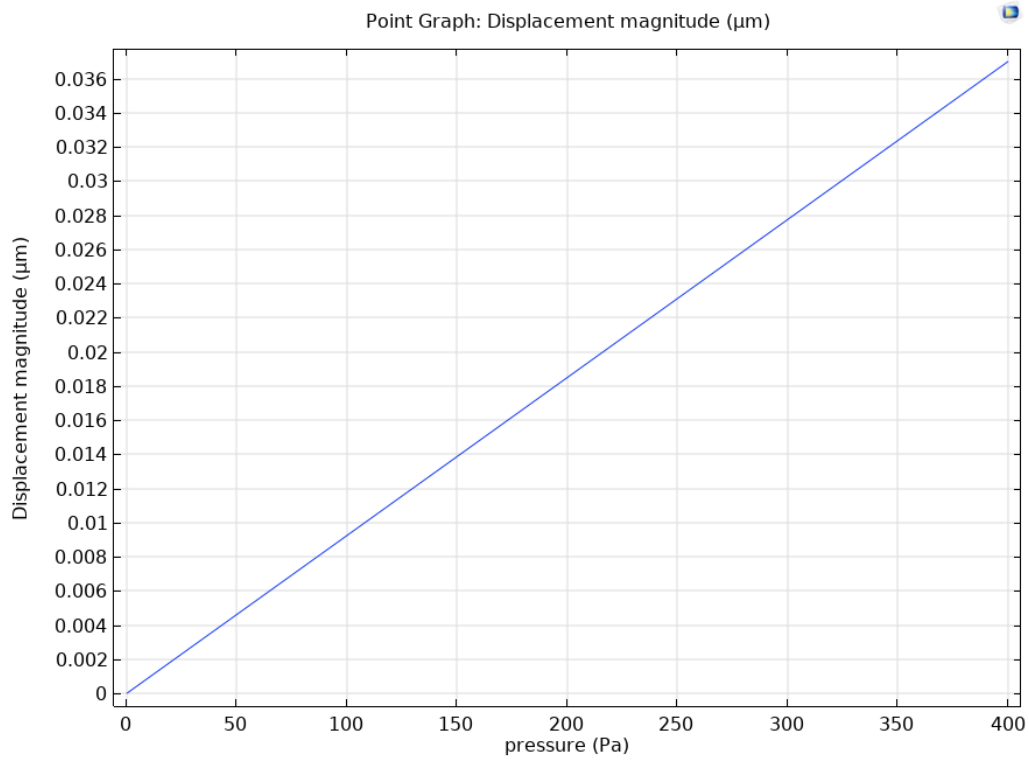


Figure 7.9: Pressure VS Displacement Analysis (Circular shape of active size element):

CHAPTER 8: CONCLUSION AND FUTURE WORK

8.1 Conclusion

This thesis introduces the design and analysis of a novel MEMS PVDF piezoelectric hydrophone with the distinct ability to detect the direction of sound waves, significantly improving its functionality for underwater applications. This directional sensing capability adds a valuable dimension to its performance, making it especially suited for tasks such as underwater navigation, target detection, and environmental monitoring. Through mathematical analyses, modeling, and simulations, it has been demonstrated that this new structure not only maintains the inherent advantages of piezoelectric sensors but also introduces directional sensitivity—a feature previously unattainable with traditional designs.

The hydrophone operates effectively at low frequencies, which is crucial for underwater sound detection, especially in the frequency range below 1.5 kHz. The performance has been significantly improved by utilizing PVDF as the piezoelectric material instead of PZT. This substitution has resulted in a sensitivity increase of 5 dB, with the hydrophone achieving a sensitivity of -186.5 dB, marking a substantial enhancement over earlier designs. The use of PVDF not only provides better flexibility and adaptability but also contributes to improved acoustic impedance matching, making the sensor more efficient in converting mechanical stress into an electrical signal, especially in low-frequency environments.

The mechanical structure of the beam further complements the sensor's performance, allowing it to be responsive to subtle pressure changes, which is essential for accurate sound wave detection and directionality. The integration of these design improvements positions this hydrophone as a more sensitive, versatile, and efficient solution compared to previous models.

Overall, this work advances the state of MEMS hydrophone design by combining PVDF material's advantages with a novel structural approach that enhances sensitivity, directional detection, and low-frequency operation. The contributions of this thesis lay the groundwork for further exploration in the field, potentially opening new avenues for underwater acoustic sensing, environmental monitoring, and naval applications.

8.2 Future Work

The initial step in future work would be the fabrication of the designed hydrophone, followed by an experimental setup to test its performance. These tests should first be performed in a controlled water tank environment, where variables such as pressure, temperature, and particle movement can be carefully regulated. Although some sensors have been tested in water tanks, the limitation of these experiments lies in their restricted frequency range, which is often influenced by the size of the tank. Therefore, the performance of the PVDF hydrophone needs to be tested not only in shallow water but also in deep-water environments, where low-frequency measurements can be conducted more effectively. In deep water, factors such as pressure changes, temperature gradients, and particle movement become more significant and must be carefully evaluated, as these elements will directly influence the hydrophone's sensitivity and accuracy.

Additionally, during the fabrication process, practical challenges such as the imperfect placement of PVDF films may arise, impacting the overall performance. The errors and uncertainties related to manufacturing need to be thoroughly analyzed, and methods for minimizing these errors should be developed. Estimation of potential errors, consideration of manufacturing tolerances, and the identification of methods to handle these uncertainties will be critical steps before deploying the hydrophone in real-world applications.

REFERENCES

- [1] H. Saheban and Z. Kordrostami, 'Hydrophones, fundamental features, design considerations, and various structures: A review', *Sens Actuators A Phys*, vol. 329, p. 112790, Oct. 2021, doi: 10.1016/J.SNA.2021.112790.
- [2] A. Hurrell, S. R.-I. T. on Ultrasonics, and undefined 2016, 'The practicalities of obtaining and using hydrophone calibration data to derive pressure waveforms', *ieeexplore.ieee.orgAM Hurrell, S RajagopalIEEE Transactions on Ultrasonics, Ferroelectrics, and Frequency, 2016•ieeexplore.ieee.org*, Accessed: Sep. 25, 2024. [Online]. Available: https://ieeexplore.ieee.org/abstract/document/7523441/?casa_token=i8Yy5nviQJEAAAAA:EufaNXW6IETxqd471S_JLa9rhWziYFV538yA0doR8CQX7DWwIMXzXqbrlKA3GRMC3B3XBkD9hno
- [3] X. Xu, Z. Zheng, L. B.-S. on Piezoelectricity, undefined Acoustic, and undefined 2014, 'Theoretical modeling and optimization design of high frequency piezoelectric polymer film hydrophone array', *ieeexplore.ieee.orgX Xu, Z Zheng, L BaiProceedings of the 2014 Symposium on Piezoelectricity, Acoustic, 2014•ieeexplore.ieee.org*, Accessed: Sep. 25, 2024. [Online]. Available: <https://ieeexplore.ieee.org/abstract/document/6998569/>
- [4] G. Zhang, P. Zhao, W. Z.-A. Advances, and undefined 2015, 'Resonant frequency of the silicon micro-structure of MEMS vector hydrophone in fluid-structure interaction', *pubs.aip.org*, Accessed: Sep. 25, 2024. [Online]. Available: <https://pubs.aip.org/aip/adv/article/5/4/041316/595812>
- [5] L. Liu, G. Zhang, ... G. C.-... C. on C., and undefined 2012, 'Design of a Novel MEMS Resonant-Column Type Bionic Vector Hydrophone', *ieeexplore.ieee.orgL Liu, G Zhang, G Chen, W Zhang2012 International Conference on Computing, Measurement, Control, 2012•ieeexplore.ieee.org*, Accessed: Sep. 24, 2024. [Online]. Available: <https://ieeexplore.ieee.org/abstract/document/6245842/>
- [6] P. C. Etter, 'Advanced Applications for Underwater Acoustic Modeling', *Adv Acoust Vib*, vol. 2012, no. 1, p. 214839, Jan. 2012, doi: 10.1155/2012/214839.

- [7] G. Zhang *et al.*, 'Design and implementation of a composite hydrophone of sound pressure and sound pressure gradient', *mdpi.com* G Zhang, L Zhang, S Ji, X Yang, R Wang, W Zhang, S Yang *Micromachines*, 2021 • *mdpi.com*, vol. 12, no. 8, Aug. 2021, doi: 10.3390/mi12080939.
- [8] R. A. Kosobrodov and V. N. Nekrasov, 'Effect of the diffraction of sound by the carrier of hydroacoustic equipment on the results of measurements', *Akusticheskij Zhurnal*, vol. 47, no. 3, pp. 382–389, 2001, doi: 10.1007/BF03353587.
- [9] P. Amiri, Z. Kordrostami, K. H.-M. Journal, and undefined 2020, 'Design of a MEMS bionic vector hydrophone with piezo-gated MOSFET readout', *Elsevier*, Accessed: Sep. 25, 2024. [Online]. Available: <https://www.sciencedirect.com/science/article/pii/S0026269219309619>
- [10] M. Liu, Z. M. Jian, G. Zhang, N. Guo, and W. Zhang, 'Design of MEMS bionic vector hydrophone based on NBR sound-transparent cap', *Sensor Review*, vol. 35, no. 3, pp. 303–309, Jun. 2015, doi: 10.1108/SR-11-2014-0744/FULL/HTML.
- [11] H. Herzog, S. Steltenkamp, A. Klein, S. Tätzner, E. Schulze, and H. Bleckmann, 'Micro-machined flow sensors mimicking lateral line canal neuromasts', *mdpi.com* H Herzog, S Steltenkamp, A Klein, S Tätzner, E Schulze, H Bleckmann *Micromachines*, 2015 • *mdpi.com*, vol. 6, no. 8, pp. 1189–1212, 2015, doi: 10.3390/mi6081189.
- [12] A. Quattieri, F. Rizzi, M. T. Todaro, A. Passaseo, R. Cingolani, and M. De Vittorio, 'Stress-driven AlN cantilever-based flow sensor for fish lateral line system', *Elsevier*, vol. 88, no. 8, pp. 2376–2378, Aug. 2011, doi: 10.1016/j.mee.2011.02.091.
- [13] G. J. Zhang, L. X. Liu, W. D. Zhang, and C. Y. Xue, 'Design of a monolithic integrated three-dimensional MEMS bionic vector hydrophone', *Microsystem Technologies*, vol. 21, no. 8, pp. 1697–1708, Aug. 2015, doi: 10.1007/S00542-014-2262-0.
- [14] L. Zhang, Q. Xu, G. Zhang, R. Wang, ... Y. P.-S. and A. A., and undefined 2019, 'Design and fabrication of a multipurpose cilia cluster MEMS vector hydrophone', *Elsevier* L Zhang, Q Xu, G Zhang, R Wang, Y Pei, W Wang, Y Lian, S Ji, W Zhang *Sensors and Actuators A: Physical*,

2019•Elsevier, Accessed: Sep. 24, 2024. [Online]. Available:
<https://www.sciencedirect.com/science/article/pii/S0924424718316753>

- [15] G.-J. Hang *et al.*, 'A bionic fish cilia median-low frequency three-dimensional piezoresistive MEMS vector hydrophone', *SpringerG Hang, Z Li, S Wu, C Xue, S Yang, W ZhangNano-Micro Letters*, 2014•Springer, doi: 10.5101/nml.v6i2.p136-142.
- [16] N. Izadi *et al.*, 'Fabrication of dense flow sensor arrays on flexible membranes', *TRANSDUCERS 2009 - 15th International Conference on Solid-State Sensors, Actuators and Microsystems*, pp. 1075–1078, 2009, doi: 10.1109/SENSOR.2009.5285945.
- [17] S. DIJKGRAAF, 'The functioning and significance of the lateral-line organs.', *Biol Rev Camb Philos Soc*, vol. 38, pp. 51–105, 1963, doi: 10.1111/J.1469-185X.1963.TB00654.X.
- [18] W. K. Metcalfe, C. B. Kimmel, and E. Schabtach, 'Anatomy of the posterior lateral line system in young larvae of the zebrafish', *Journal of Comparative Neurology*, vol. 233, no. 3, pp. 377–389, 1985, doi: 10.1002/CNE.902330307.
- [19] P. Morse and K. Ingard, *Theoretical acoustics*. 1986. Accessed: Sep. 25, 2024. [Online]. Available:
[https://books.google.com/books?hl=en&lr=&id=KIL4MV9IE5kC&oi=fnd&pg=PR7&dq=3.+Dijkgraaf+S+\(1963\)+The+1.%09Morse,+P.M.%3B+Ingard,+K.U.+Theoretical+Acoustics.+McGraw-Hill:+New+York,+NY,+USA,+1968and+significance+of+the+lateral+line+organs.+Biol+Rev+38:51%E2%80%93105.+doi:10.1111/j.1469-185X.1963.+tb00654.x&ots=hnKjAdRiE_&sig=FeKVTwYO2SszZojr2Wr1WdmuXtjw](https://books.google.com/books?hl=en&lr=&id=KIL4MV9IE5kC&oi=fnd&pg=PR7&dq=3.+Dijkgraaf+S+(1963)+The+1.%09Morse,+P.M.%3B+Ingard,+K.U.+Theoretical+Acoustics.+McGraw-Hill:+New+York,+NY,+USA,+1968and+significance+of+the+lateral+line+organs.+Biol+Rev+38:51%E2%80%93105.+doi:10.1111/j.1469-185X.1963.+tb00654.x&ots=hnKjAdRiE_&sig=FeKVTwYO2SszZojr2Wr1WdmuXtjw)
- [20] A. Pierce, *Acoustics: an introduction to its physical principles and applications*. 2019. Accessed: Sep. 25, 2024. [Online]. Available:
https://books.google.com/books?hl=en&lr=&id=MAGfDwAAQBAJ&oi=fnd&pg=PR10&dq=2.%09Pierce,+A.D.+Acoustics%F4%80%8A%8AA+Introduction+to+Its+Physical+Principles+and+Applications.+McGraw-Hill:+New+York,+NY,+USA,+1981.&ots=T_Ina_70UE&sig=CYxeccrhImoj3FanBg3FfHw_Fl8

- [21] A. Nehorai, E. P.-I. T. on signal processing, and undefined 1994, 'Acoustic vector-sensor array processing', *ieeexplore.ieee.org* A Nehorai, E Paldi *IEEE Transactions on signal processing*, 1994 • *ieeexplore.ieee.org*, Accessed: Sep. 25, 2024. [Online]. Available: https://ieeexplore.ieee.org/abstract/document/317869/?casa_token=EtaPhKVgBSkAAAAA:-YTIzdmGs7Z0Z5lzSM3GvWJJriHBF20GRoywzyWudlb3LxQAT_0ee0s6NHUfqewd2_fUHmQezE
- [22] S. Sukumaran, S. Chatbouri, D. Rouxel, E. Tisserand, F. Thiebaud, and T. Ben Zineb, 'Recent advances in flexible PVDF based piezoelectric polymer devices for energy harvesting applications', *J Intell Mater Syst Struct*, vol. 32, no. 7, pp. 746–780, Apr. 2021, doi: 10.1177/1045389X20966058.
- [23] M. Younis, *MEMS linear and nonlinear statics and dynamics*. 2011. Accessed: Sep. 25, 2024. [Online]. Available: https://books.google.com/books?hl=en&lr=&id=5wznpjKOsmiQC&oi=fnd&pg=PR2&dq=MEMS+LINEAR+AND+NON+LINEAR+STATICS+AND+DYNAMICS&ots=svthgk_ugZ&sig=ot86AB6egtb tGoNaMLA0bl37Vdk
- [24] S. D. Senturia, *Microsystem design*. 2005. Accessed: Sep. 25, 2024. [Online]. Available: [https://books.google.com/books?hl=en&lr=&id=UY3wBwAAQBAJ&oi=fnd&pg=PT23&dq=Senturia+S+D+\(2001\)+Microsystem+design.+Springer,+NewYork&ots=I6E_RcxEtp&sig=FgzTD1Gc KdTPwDFpvMEPWsT3Fkw](https://books.google.com/books?hl=en&lr=&id=UY3wBwAAQBAJ&oi=fnd&pg=PT23&dq=Senturia+S+D+(2001)+Microsystem+design.+Springer,+NewYork&ots=I6E_RcxEtp&sig=FgzTD1Gc KdTPwDFpvMEPWsT3Fkw)
- [25] A. Preumont, *Dynamics of electromechanical and piezoelectric systems*. 2006. Accessed: Sep. 25, 2024. [Online]. Available: <https://link.springer.com/content/pdf/10.1007/1-4020-4696-0.pdf>
- [26] C. H. Sherman and J. L. Butler, *Transducers and arrays for underwater sound*. 2007. Accessed: Sep. 25, 2024. [Online]. Available: <https://link.springer.com/content/pdf/10.1007/978-0-387-33139-3.pdf>

- [27] O. Lotsberg, J. Hovem, ... B. A.-J. of the A. S. of, and undefined 1996, 'Experimental observation of subharmonic oscillations in Infoson bubbles', *pubs.aip.org*, Accessed: Sep. 25, 2024. [Online]. Available: <https://pubs.aip.org/asa/jasa/article-abstract/99/3/1366/751822>
- [28] L. De Medeiros, ... H. K.-M., and undefined 2015, 'Piezoelectret-based hydrophone: An alternative device for vibro-acoustography', *iopscience.iop.org*, 2015, doi: 10.1088/0957-0233/26/9/095102.
- [29] S. Choi, H. Lee, W. M.-S. and A. A. Physical, and undefined 2010, 'A micro-machined piezoelectric hydrophone with hydrostatically balanced air backing', *ElsevierS Choi, H Lee, W MoonSensors and Actuators A: Physical, 2010•Elsevier*, Accessed: Sep. 25, 2024. [Online]. Available: <https://www.sciencedirect.com/science/article/pii/S0924424709005457>

LIST OF PUBLICATIONS AND PATENTS

- Industrial Design Patent Application Titled “Temperature Sensor Array” submitted on 19 Aug 2024.